別紙様式１（論文博士申請者用）

博 士 学 位 論 文

Neuromuscular physiology research to address age-related decline in physical function

加齢に伴う身体機能低下に対処する神経筋生理学研究

（西暦）　2024 年　1 月　5 日　提出

東京都立大学大学院
人間健康科学研究科　人間健康科学専攻
ヘルスプロモーションサイエンス学域
客員研究員受入通知書の文書番号: ４都立大荒管第９５６号
氏　名：田村　晃太郎

（指導/紹介教員名：　藤井　宣晴　）

CONTENTS

ABSTRACT

Age-related decline in physical function and muscle atrophy are significant challenges to the health and well-being of older adults. This doctoral thesis presents a series of experiments aimed at elucidating the underlying mechanisms and proposing potential countermeasures for preventing the decline in physical function caused by aging. Experiment #1 focused on investigating skeletal muscle factors contributing to maintain muscle mass. The study demonstrated that tyrosine in combination with leucine enhanced anabolic signals, thereby promoting protein synthesis in skeletal muscle. Experiments #2 and #3 focused on neurological factors influencing age-related muscle weakness. The studies explored the effects of cutaneous stimulation on spinal motor control and motor neuron excitability during exercise. The results indicated that low-load exercise with TRPM8-mediated skin cooling promoted preferential recruitment of large motor neurons, which were innervating the type 2 myofibers. The repetitive exercise intervention enhanced the spinal excitatory inputs to motor neurons, thereby contributing to physical improvement in aged mice. Collectively, these experiments shed light on the interplay between neurological and skeletal muscle factors to address age-related physical dysfunction. The findings from experiment #1 suggest that targeting specific amino acids could provide an effective nutritional intervention for preventing muscle atrophy. Experiments #2 and #3 suggest that exercise with TRPM8-mediated skin cooling is a potential training method for rehabilitation or preventive measures in long-term care for older adults. The insights obtained from these experiments should be applied to the development of integrative countermeasures to prevent age-related decline in physical function and muscle atrophy.

ABBREVIATIONS, KEYWORDS

ABBREVIATIONS

MPS: muscle protein synthesis; mTORC1: mammalian target of rapamycin complex 1; S6K: S6 kinase; 4E-BP: eukaryotic translation initiation factor 4E-binding protein; EAAs: essential amino acids; SUnSET: surface sensing of translation; EDL: extensor digitorum longus; MNs: motor neurons; MU: motor unit; INs: interneurons; TRPM8: transient receptor potential channel sub-family M8; SC: skin cooling; HU: hindlimb unloading; ChAT: choline acetyltransferase; VAChT: vesicular acetylcholine transporter; VGLUT1: vesicular glutamate transporter 1.

KEYWORDS

skeletal muscle, amino acid, Sestrin, spinal cord, motor neuron, C-bouton, TRPM8

CHAPTER 1. GENERAL INTRODUCTION

The decline in physical function and muscle atrophy with aging is a major public health concern. The mechanisms accounting for a decrease in muscular strength can arise from two broad categories: neurological and skeletal muscle factors (1). The neuromuscular system contains several components that affect maximal voluntary force, such as excitatory drive from supraspinal centers, motor neuron excitability, antagonistic muscle activity, motor unit recruitment and rate coding, neuromuscular transmission, muscle mass, E-C coupling processes, and muscle morphology and architecture. Both the neurological and muscular factors potentially contribute to the age-related loss of muscle strength and power. To address these concerns, this doctoral thesis is comprised of three experiments focused on the underlying mechanisms of skeletal muscle factors (experiment #1) and neurological factors (experiment #2 and #3).

CHAPTER 2. LITERATURE REVIEW

Skeletal muscle atrophy from motor neuron's perspective

Skeletal muscle atrophy appears to be inevitable with aging. A gradual loss of muscle fibers begins at around age 50, and by the age of 80s, approximately 50% of the fibers are lost from the limb muscles (2), as well as 30-50% of the muscle mass (3,4). Skeletal muscle mass is particularly lost in the lower limbs than in the upper limbs (5). Skeletal muscle atrophy is also closely associated with a decrease in muscle strength and power (6), which is mainly cause by decreasing the size and the number of fast-twitch (type 2) muscle fibers. The cross-sectional area of type 2 muscle fibers decreases with aging, whereas that of slow-twitch (type 1) fibers remains unaffected by aging (3,7). Although several hypotheses have been considered to explain why type 2 muscle fibers are lost with aging, the main cause is a decrease in motor neurons (MNs). There are very few reports in humans on changes in the number of MNs with aging: a rapid decrease in MNs is observed after the age of 60s (8), and the age of 60s has approximately 25-50% fewer MNs compared to the 20s (9). Consequently, motor units consisting of a MN and the skeletal muscle fibers it innervates are apparently lost after the age of 60s. In young adults, loss of MNs through either injury or disease results in the remaining healthy MNs sprouting to innervate the denervated fibers. This capacity for sprouting is impaired in the hindlimb muscles with aging (10). The reasons for decreasing MNs and motor units with aging remains unclear, but it is predicted to involve reduced activity in the motor cortex, increased oxidative stress in MNs, local degeneration at axon terminals, and feedback signals from impaired energy metabolism of muscle fibers (11).

Regulation of muscle protein synthesis

Skeletal muscle is constantly maintained by muscle protein synthesis (anabolism) and degradation (catabolism). The difference between protein synthesis and degradation in skeletal muscle is called net balance, and muscle mass increases only when the rate of protein synthesis exceeds the rate of protein degradation. The net balance is negative during fasting (resting state), but the rate of muscle protein synthesis (MPS) after feeding doubles compared to the resting state, thereby the net balance turns positive (12). Diet-induced anabolic responses in skeletal muscle occur primarily through protein ingestion. Protein is taken up into the blood as amino acids. The amino acids are taken up by skeletal muscle as the increase of amino acids concentration in the blood. The intracellular free amino acids increased in muscle cells then promotes MPS. Exercise is another stimulus for MPS. A single bout of resistance training exercise keeps MPS up to about 48 hours after exercise (13). In contrast, when resistance exercise is performed during fasting, muscle degradation is simultaneously enhanced (14). Thus, ingesting amino acids or protein immediately after resistance exercise increases the concentration of amino acids in the blood, that inhibit muscle protein degradation, thereby effectively enhancing MPS (15).

Recent studies have reported that MPS in older adults is less responsive to amino acids and exercise, termed "anabolic resistance" (16). It is possible that the proportion of ingested amino acids consumed in the gastrointestinal tract and liver increases with aging, and that enough amino acids are not supplied to peripheral tissues including skeletal muscle (17,18). Second, insulin resistance in skeletal muscle may be another factor. Insulin is also an anabolic stimulus for MPS (19,20). However, MPS does not promote with insulin administration in older adults, presumably due to insulin resistance in skeletal muscle (21). Third, mammalian target of rapamycin complex 1 (mTORC1) signal regulating MPS in muscle cells is less

responsive to resistance exercise in older adults (22), suggesting that the intracellular signal pathways that contribute to MPS are impaired. Notably, the baseline of mTORC1 phosphorylation state in skeletal muscle in overnight-fasting older adults is higher compared to young adults (23). Disturbances in proteasomal degradation and autophagy in muscles may be linked to increased mTORC1 activity when aged mice were subjected to fasting (24). Thus, the finely controlled mTORC1 activity must be impaired in aged skeletal muscle. This may cause the attenuative response of MPS by amino acids and exercise.

CHAPTER 3. GENERAL PURPOSE

This doctoral thesis aims to understand the mechanisms regulating muscle anabolic response and motor unit recruitment and to develop integrative countermeasures to prevent age-related decline in physical function and muscle atrophy.

CHAPTER 4. EXPERIMENT #1

Tyrosine is a booster of leucine-induced muscle anabolic response

CHAPTER 4-1. INTRODUCTION

Skeletal muscle mass is maintained through a balance between protein synthesis and degradation. Nutritional supplementation with proteins or amino acids activates anabolic responses in the skeletal muscle and may be important for counteracting muscle loss due to aging, sarcopenia, or frailty (25,26). The intracellular signaling mechanism regulating muscle protein synthesis (MPS) is controlled by the activation of the mammalian target of rapamycin complex 1 (mTORC1), which directly stimulates the phosphorylation of S6 kinase (S6K) and eukaryotic translation initiation factor 4E-binding protein (4E-BP). Changes in the phosphorylation state of these key proteins affect mRNA translation initiation and elongation, thereby regulating MPS (27). Essential amino acid (EAA) supplementation effectively stimulates MPS; however, non-essential amino acids (NEAAs) are ineffective even at significantly high doses (28,29). Among EAAs, leucine (Leu) is particularly important for MPS, as it is the only stimulator of mTORC1 signaling identified in muscle cells over the physiological range of amino acid levels in blood (30). The amount of Leu in ingested proteins or EAA mixtures determines the extent of the MPS response at rest and after exercise (31–34). The amino acid composition of whey protein is suitable for stimulating MPS, owing to its high Leu content and absorbability (35,36). Thus, Leu is widely accepted as being indispensable for stimulating mTORC1 signaling. Recently, the mechanism underlying Leu-mediated mTORC1 activation was elucidated using HEK293T cells (37,38). In these studies, mTORC1 regulation by amino acids was found to be mediated by Rag guanosine triphosphatase (GTPase) via several factors,

including GATOR1, a GTPase-activating protein that inhibits mTORC1 in response to amino acid starvation, GATOR2, which inhibits GATOR1 activity, and Sestrin2, a GATOR2-interacting protein (39,40). Leu disrupts the Sestrin2–GATOR2 inter-action by binding to Sestrin2, and GATOR2 in turn activates mTORC1 by binding to GATOR1 (37,38). Although three Sestrin isoforms, 1–3, are expressed in mammalian cells, Leu promotes only the dissociation of Sestrin1 and Sestrin2 from GATOR2 (37). In skeletal muscle, Leu-mediated mTORC1 activation occurs primarily through Sestrin1 rather than Sestrin2, as Sestrin1 is more highly expressed than Sestrin2 (41).

Though Leu is undoubtedly important for MPS, recent studies have revealed several mechanisms related to other EAAs, including glutamine (42), arginine (43), and methionine (44), underlying mTORC1 activation. However, to the best of our knowledge, the intrinsic contribution of other amino acids, including NEAAs, to Leu-mediated activation of mTORC1 signaling has not yet been assessed. This experiment aimed to identify amino acids that play a role in enhancing Leu-mediated activation of mTORC1 signaling in skeletal muscle. Collectively, our data provide novel insights into the most appropriate composition of daily protein/amino acid macronutrients or supplements.

CHAPTER 4-2. MATERIALS AND METHODS

4-2-1. Cell Culture and Treatments

C2C12 myoblasts (European Collection of Authenticated Cell Cultures, Salisbury, UK) were seeded at a density of 1.25×10^5 cells/well in 8-well rectangular plates and maintained in Dulbecco's Modified Eagle's medium (DMEM; 25 mM glucose; Sigma, St. Louis, MO, USA) supplemented with 10% fetal bovine serum (FBS; Biosera, Kansas City, MO, USA) and 1% penicillin–streptomycin (PS; Life Technologies, Carlsbad, CA, USA) at 37 °C in a 5% CO_2-containing atmosphere. At 80% confluence, the culture medium was changed to a differentiation medium consisting of DMEM supplemented with 2% horse serum (HS; Life Technologies) and 1% PS (day 0). The cells were collected and used for western blotting and the evaluation of myotube hypertrophy on days 1 and 5 post-differentiation, respectively. The cells were deprived of serum and amino acids through incubation in Hanks' Balanced Salt Solution (HBSS with Ca and Mg, without Phenol Red; Life Technologies) for 3–4 h; this was followed by inoculation with various amino acids for 10–30 min. Amino acids used for the cell experiments were purchased from Fuji-film Wako (Osaka, Japan).

4-2-2. siRNA Transfection

To deliver oligonucleotide-based siRNAs (Silencer Select pre-designed siRNA; Thermo Fisher Scientific, Waltham, MA, USA) into cells, 50–60% confluent C2C12 cells were transfected with 10 nM siRNA using lipofectamine RNAiMAX (Invitrogen) and Opti-MEM I Reduced-Serum Medium (Invitrogen), according to the instructions of the manufacturer. The culture medium was changed to a differentiation medium 24 h after transfection, and the cells were collected and used for experiments on

day 1 post-differentiation. The siRNAs used in this study were the Silencer Negative Control #2, Sestrin1 (s100521), Sestrin2 (s100521), and Leucyl-tRNA Synthetase (LRS, s98763) siRNAs.

4-2-3. Evaluation of Amino Acid-Induced S6K Phosphorylation

C2C12 myoblasts were seeded at a density of 6×10^4 cells/well in 96-well plates and cultured at 37 °C and in a 5% CO_2-containing environment overnight. The following day, the medium was replaced with HBSS, and the cells were cultured for 3–4 h. Subsequently, the cells were incubated with various concentrations of amino acids for 15 min. After removal of HBSS, the cells were lysed using CelLytic MT Cell Lysis Reagent (C3228; Sigma) for 10 min, and the extract was subjected to an AlphaScreen SureFire assay (TGR70S500; PerkinElmer, Waltham, MA, USA) to detect phospho-p70 S6K (Thr 389) following the instructions of the manufacturer. The values were corrected for protein concentrations determined separately using a Pierce BCA Protein Assay Kit (Thermo Fisher Scientific). All data are presented relative to those of control-deprived amino acids.

4-2-4. Immunohistochemistry and Evaluation of Myotube Hypertrophy

C2C12 myoblasts were cultured for five days in a differentiation medium supplemented with Leu and/or tyrosine (Tyr). During this period, the medium was changed daily. On day 5 post-differentiation, C2C12 myotubes were washed with PBS and fixed with 4% paraformaldehyde PBS (Fujifilm-Wako) for 20 min at 4 °C. The fixed cells were washed thrice with PBS and incubated with 0.2% TritonX-100 (Sigma) in PBS for 10 min at room temperature (RT). After incubation in a blocking solution (3% BSA, Sigma; in PBS) for 30 min at RT, the cells were incubated with primary antibodies against the Myosin heavy chain (MyHC, MF 20sp; DSHB, Iowa City, IA, USA), diluted in the blocking solution to 5 μg/mL, at 4 °C overnight. After the cells were washed in PBS, they were incubated with secondary antibodies (Alexa 488-

conjugated donkey anti-mouse antibodies (1:500, Molecular Probes, Thermo Fisher Scientific)) diluted in the blocking solution for 1 h at RT. The cells were subsequently washed with PBS and stained with DAPI (Dojindo, Kumamoto, Japan). Images of the stained cells were captured using an all-in-one fluorescence micro-scope (BZ-X710; Keyence, Osaka, Japan) at a magnification of 10×. The average myotube diameter was calculated as the mean of three measurements taken along the long axis of the myotubes using a BZ Analyzer (Keyence); in total, 133–142 myotubes were evaluated from four random fields.

4-2-5. Animals and Diets

Male C57BL/6J mice were purchased from CLEA Japan (Tokyo, Japan) and maintained under controlled conditions (temperature: 23 ± 2 °C; humidity: 55 ± 10%; lighting: 07:00 to 19:00 h). The mice were provided standard chow (CE-2; CLEA Japan, Tokyo, Japan) and ad libitum access to water. All animal experiments were conducted at the Experimental Animal Facility of the Kao Tochigi Institute (Tochigi, Japan) and were approved by the Animal Care Committee of the Kao Corporation (Tokyo, Japan). Food additive-grade L-Leu and L-Tyr used in the animal experiments were purchased from Ajinomoto Healthy Supply (Tokyo, Japan).

4-2-6. Animal Experiment 1: Incubation of Isolated Muscles

Overnight-fasted mice (14 weeks old, n = 20) were sacrificed, and their soleus and the extensor digitorum longus (EDL) muscles were removed from both hindlimbs. Two muscles isolated from both legs of one mouse were independently used in the experiment. The isolated soleus and EDL muscles (n = 40 each) were randomly assigned to one of six treatment groups. The incubation of the isolated muscles was performed as previously described (45), with slight modifications. Briefly, isolated muscles tied with silk thread at both tendon ends were mounted on an incubation apparatus and pre-incubated in Krebs Ringer

Bicarbonate (KRB) buffer (K4002, Sigma) for 10 min. Thereafter, the buffer was replaced with a fresh KRB buffer supplemented with Leu and/or Tyr. In addition, 95% O_2-5% CO_2 was continuously bubbled through the buffer at 37 °C. After 20 min of incubation, the isolated muscles were washed with ice-cold KRB buffer and stored at −80 °C until further analyses.

4-2-7. Animal Experiment 2: Oral Administration of Amino Acids

Overnight-fasted mice (8 weeks old, n = 51) with similar average body weights were randomly assigned to one of the seven dietary treatments. The control group received an emulsion containing 2 g of fat per kg of body weight (BW), and the treatment groups received the same amount of emulsion with either Leu at 5 mmol/kg BW, Leu at 10 mmol/kg BW, Tyr at 1 mmol/kg BW, Tyr at 5 mmol/kg BW, Leu at 5 mmol/kg BW + Tyr at 1 mmol/kg BW, or Leu at 5 mmol/kg BW + Tyr at 5 mmol/kg BW. The maximum amount of Leu (10 mmol/kg BW), which was the equivalent of the amount of Leu consumed by rats per day, was determined based on data from previous studies (46,47). Glyceryl trioleate (Sigma) was used as a fat source. Lecithin from egg yolk (Kanto Chemical, Tokyo, Japan) was added to all test emulsions at 0.08 g/kg BW (0.4% (w/w)) in the administered samples. Premixed solutions were subsequently sonicated thrice for 60 s, with a 1 min interval of cooling on ice, to obtain stable emulsions (Sonifier 450; Branson Ultrasonics, Danbury, CT, USA), as previously described (48). The lipid emulsion was intragastically administered to mice under isoflurane anesthesia at a dose of 20 mL/kg BW (Abbott Laboratories, Chicago, IL, USA), and then the mice were returned to their cages. Thirty minutes after amino acid administration, blood samples were collected from the abdominal venae cavae of the mice under isoflurane anesthesia, and the mice were sacrificed. The muscles were collected from both mouse hindlimbs and stored at −80 °C until

analysis. The collected blood samples were preserved on ice and centrifuged at 10,000× g for 6 min at 4 °C, and mouse sera were stored at −80 °C until analysis.

4-2-8. Western Blotting

Cells or frozen muscle samples were homogenized in the CelLytic MT Cell Lysis Reagent (Sigma) supplemented with a complete protease inhibitor cocktail (Roche, Basel, Switzerland) and a phosphatase inhibitor cocktail solution (Fujifilm-Wako) using an ultrasonic homogenizer (Sonifier 150; Branson Ultrasonics) or a handy micro homogenizer (PHYSCOTRON, NS-310E3; MICROTEC, Chiba, Japan), respectively. After centrifugation at 13,500× g for 15 min at 4 °C, the protein concentration of the supernatant was determined using the Pierce BCA Protein Assay Kit. Samples were separated on an SDS-polyacrylamide gel (10% or 4–15% Mini-PROTEAN TGX Gels; Bio-Rad, Hercules, CA, USA) and transferred onto polyvinylidene fluoride (PVDF) membranes (ClearTrans SP; Fujifilm-Wako). The membranes were then blocked with a PVDF blocking reagent (TOYOBO, Osaka, Japan). Subsequently, the membranes were incubated overnight with anti-S6K (9202; Cell Signaling Technology (CST), Danvers, MA, USA), anti-P-S6K (Thr389, 9205; CST), anti-4E-BP (9452; CST), anti-P-4E-BP (Thr37/46, 2855; CST), anti-mTOR (2972; CST), anti-P-mTOR (Ser2448, 2971; CST), anti-P-S6 (Ser235/236, 2211; Ser240/244, 2215; CST), anti-S6 (2217; CST), anti-GAPDH (2118, CST), anti-LRS (13868, CST), anti-Sestrin1 (21668-1-AP, Proteintech, Rosemont, IL, USA), and anti-Sestrin2 (10795-1-AP, Proteintech) antibodies, diluted at a 1:2000 ratio using an immunoreaction-enhancing solution (Can Get Signal, TOYOBO). The appropriate secondary antibodies conjugated with horseradish peroxidase (7074; CST, dilution 1:2000) were used to detect blots via enhanced chemiluminescence on the ECL Prime (GE Healthcare, Chica-go, IL, USA). Images of the blots were captured using a ChemiDoc MP Imaging System

(Bio-Rad), and band volumes were adjusted with local background subtraction using the Image Lab software (Bio-Rad).

4-2-9. Muscle Protein Synthesis

Muscle protein synthesis was evaluated using the surface sensing of translation (SUnSET) method (49,50). C2C12 myoblasts (day 1) were incubated with 1 μM puromycin (Abcam, Cambridge, UK) and amino acids in HBSS buffer at 37 °C for 30 min. Then, the cells were collected and subjected to western blotting following the method described in **4-2-8**. Anti-puromycin antibodies (MABE343; Millipore, Burlington, MA, USA) were used to detect puromycin incorporation in de novo proteins. The intensities of all puromycin-labeled protein bands were normalized to that of Coomassie blue staining (Bio-Safe G-250; Bio-Rad) in each lane.

4-2-10. Measurement of Amino Acid Levels

The serum or muscle samples were homogenized using three times the volume of 15% sulfosalicylic acid (Fujifilm-Wako), and the homogenate was centrifuged at 10,000× g for 10 min at 4 °C to remove proteins. Then, the supernatant was subjected to subsequent analyses. Free Leu and Tyr levels in the samples were determined using an incorporated LC-MS/MS system (Infinity 1290; Agilent, Santa Clara, CA, and the QTRAP system; AB Sciex, Tokyo, Japan) with a Scherzo SS-C18 column (Imtakt, Kyoto, Japan). Mobile phase A consisted of 0.1 M ammonium formate in Milli-Q water, and mobile phase B consisted of 0.3% formic acid in MeOH. The initial eluent was composed of 1% B, followed by a linear increase to 90% B within 3 min. This proportion was maintained for 1 min; then, the mobile phase was returned to the initial condition and maintained for 1 min until the end of the run. The total running time was 5 min, eluent flow was 1 mL/min, and column temperature was set at 40 °C. Mass spectroscopic detection and quantification

of the analytes were performed using a multiple-reaction-monitoring (MRM) scan device in positive ion mode. Q1 and product ion scans were acquired by infusing the sample solutions of each analyte with a mixed mobile phase solution using an infusion pump. The source temperature and gas parameters were optimized after the chromatographic conditions were fixed as follows: curtain gas: 20 psi; collision gas: 8 psi; ion spray voltage: 5000 V; source temperature: 600 °C; ion source gas 1: 65 psi; ion source gas 2: 30 psi. The ionization parameters of the analytes were as follows: for Leu: declustering potential (DP): 51 V; entrance potential (EP): 10 V; collision energy (CE): 19 V; and collision cell exit energy (CXE): 36 V; for Tyr: DP: 56 V; EP: 10 V; CE: 15 V; and CXE: 22 V. The analytes were detected in a MRM mode by monitoring the characteristic fragmentation ions (m/z 132.14 > 86.3) for Leu and (m/z 182.11 > 91.1) for Tyr.

4-2-11. RNA Extraction and RT-PCR

Total RNA was extracted from C2C12 cells using an RNeasy Mini Kit (Qiagen, Hilden, Germany), following the protocol of the manufacturer. RNA was transcribed into cDNA using a high-capacity RNA-to-cDNA Kit (Applied Biosystems, Foster City, CA, USA). Quantitative RT-PCR was performed using the ABI Prism 7500 device with TaqMan gene expression assays (Applied Biosystems). The mRNA levels of each gene were normalized to the average of those of two housekeeping genes, 18S ribosomal RNA (18S rRNA) and glyceraldehyde 3-phosphate dehydrogenase (GAPDH). The probes used in this study included Mm01185732_m1 for Sestrin1, Mm00460679_m1 for Sestrin2, Mm03928990 for 18S rRNA, and Mm99999915_g1 for GAPDH.

4-2-12. Statistical Analysis

All data are presented as mean ± standard error (SE). Differences between multiple groups were tested using one-way ANOVA followed by Tukey's post-hoc test. Comparison of two factors was performed using two-way ANOVA followed by Tukey's post hoc test when a significant main effect or interaction was observed. Correlation analysis was performed using the Pearson's correlation coefficient. The threshold for significance was set at $p < 0.05$. All analyses were performed using the Prism 8 statistical software (GraphPad Software, San Diego, CA, USA).

CHAPTER 4-3. RESULTS

4-3-1. Tyr Enhanced Leu-induced Muscle Anabolic Signaling and Muscular Hypertrophy in C2C12 Cells

To verify which amino acid enhanced Leu-induced anabolic signaling, murine C2C12 myoblasts were simultaneously exposed to Leu (2.5 mM) and other amino acids (2.5 mM) for 15 min. S6K phosphorylation (Thr 389) significantly increased in response to treatment with 2.5 mM Leu + 2.5 mM Tyr or Phe, compared with that in response to treatment with 5 mM Leu (Figure 1A). Both the Leu + Tyr and Leu + Phe treatments significantly increased S6K phosphorylation in a dose-dependent manner, although the Leu + Tyr treatment possibly induced a more significant effect (Figure 1B). Therefore, we investigated the booster effect of Tyr on Leu in subsequent experiments. At concentrations ranging from 0.25 to 2.5 mM, Tyr enhanced Leu-induced S6K phosphorylation in a dose-dependent manner (Figure 1C). Although Tyr alone exerted no effect on S6K phosphorylation, the Leu + Tyr combination induced significant S6K phosphorylation at a lower Leu concentration than when Leu was administered alone (Figure 1D,E). A similar trend was observed in the activation of other signaling pathways by mTORC1-related proteins, including 4E-BP, mTOR, and S6 (Figure 1F–I). The phosphorylation of proteins related to these pathways was mainly observed 10–30 min following amino acid exposure (Figure S1A–C).

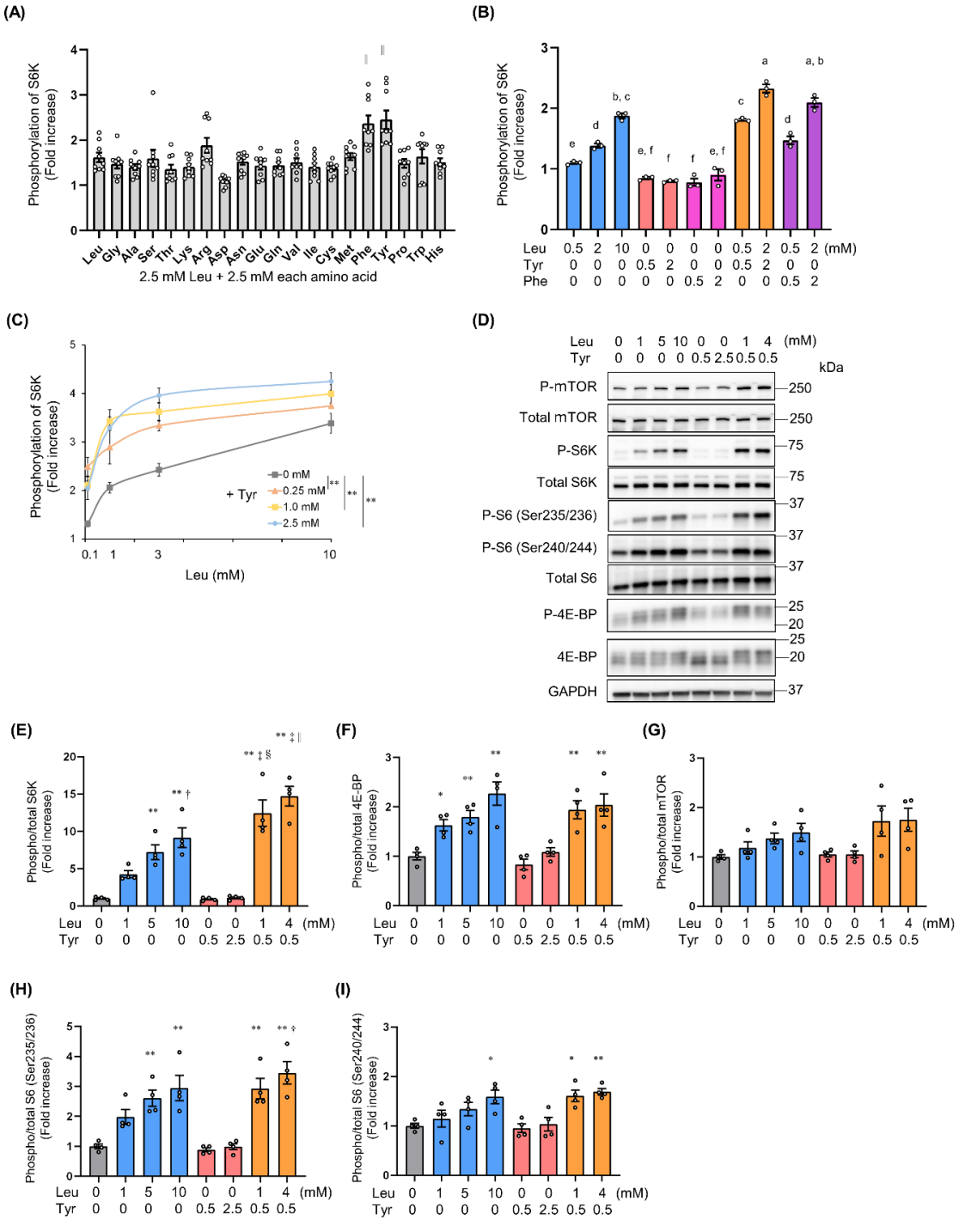
(A)
Phosphorylation of S6K (Fold increase)
Leu Gly Ala Ser Thr Lys Arg Asp Asn Glu Gln Val Ile Cys Met Phe Tyr Pro Trp His
2.5 mM Leu + 2.5 mM each amino acid
(B)
Phosphorylation of S6K (Fold increase)
Leu 0.5 2 10 0 0 0 0 0.5 2 0.5 2 (mM)
Tyr 0 0 0 0.5 2 0 0 0.5 2 0 0
Phe 0 0 0 0 0 0.5 2 0 0 0.5 2
(C)
Phosphorylation of S6K (Fold increase)
0 mM
0.25 mM
1.0 mM
2.5 mM
+ Tyr
Leu (mM)
(D)
Leu 0 1 5 10 0 0 1 4 (mM)
Tyr 0 0 0 0 0.5 2.5 0.5 0.5
kDa
P-mTOR
Total mTOR
P-S6K
Total S6K
P-S6 (Ser235/236)
P-S6 (Ser240/244)
Total S6
P-4E-BP
4E-BP
GAPDH
(E)
Phospho/total S6K (Fold increase)
(F)
Phospho/total 4E-BP (Fold increase)
(G)
Phospho/total mTOR (Fold increase)
(H)
Phospho/total S6 (Ser235/236) (Fold increase)
(I)
Phospho/total S6 (Ser240/244) (Fold increase)

Figure 1. Tyrosine enhances leucine-induced S6K phosphorylation in C2C12 myoblasts.

(A) S6K phosphorylation (Thr389) after 15 min of stimulation with 2.5 mM Leu and 2.5 mM of each amino acid (n = 9) as detected through the alpha screen assay. (B) S6K phosphorylation in response to treatment with Leu and/or Tyr or Phenylalanine (Phe) (n = 3) as detected through the alpha screen assay. (C) Dose–response evaluation of S6K phosphorylation at Leu and Tyr concentrations ranging from 0 to 10 mM and from 0 to 2.5 mM (n = 3), respectively, as detected through the alpha screen assay. (D) Representative images of anabolic signaling pathways detected in myoblasts on day 1 post-differentiation through western blotting following 15 min of stimulation with Leu and/or Tyr. Phosphorylation ratios for S6K (Thr 389) (E), 4E-BP (Thr37/46) (F), mTOR (Ser2448) (G), and S6 (Ser235/236, Ser 240/244) (H,I) were calculated by dividing the phosphorylation levels by the protein expression levels (n = 4). All data represent the fold change with respect to the control (0 mM Leu and 0 mM Tyr). Data are presented as mean ± SEM. Circles represent individual values. * $p < 0.05$, ** $p < 0.01$ vs. control † $p < 0.05$, ‡ $p < 0.01$ vs. 1 mM Leu. § $p < 0.05$, || $p < 0.01$ vs. 5 mM Leu as determined by one-way ANOVA (A,E–I). Different letters (a–f) represent significant differences ($p < 0.05$) as determined by one-way ANOVA (B). ** $p < 0.01$ vs. the Leu alone condition as determined by two-way ANOVA (C).

The SUnSET assay was used to detect incorporated puromycin in de novo proteins and demonstrated a significant increase in the protein synthesis rate in response to treatment with 5 mM Leu and the Leu + Tyr combination, i.e., 1 mM Leu + 0.5 mM Tyr and 4 mM Leu + 0.5 mM Tyr (Figure 2A,B). C2C12 cells were found to differentiate in the presence of Leu and/or Tyr, and the diameter of the myotube short axis and total protein content were quantified on day 5 post-differentiation (Figure 2C). Myotube diameter

increased following the addition of amino acids, particularly following the addition of 0.5 mM Tyr to 1 mM Leu (Figure 2D). The total protein quantity significantly increased in the Leu and Tyr combination group versus in the control and 1 mM Leu groups (Figure 2E).

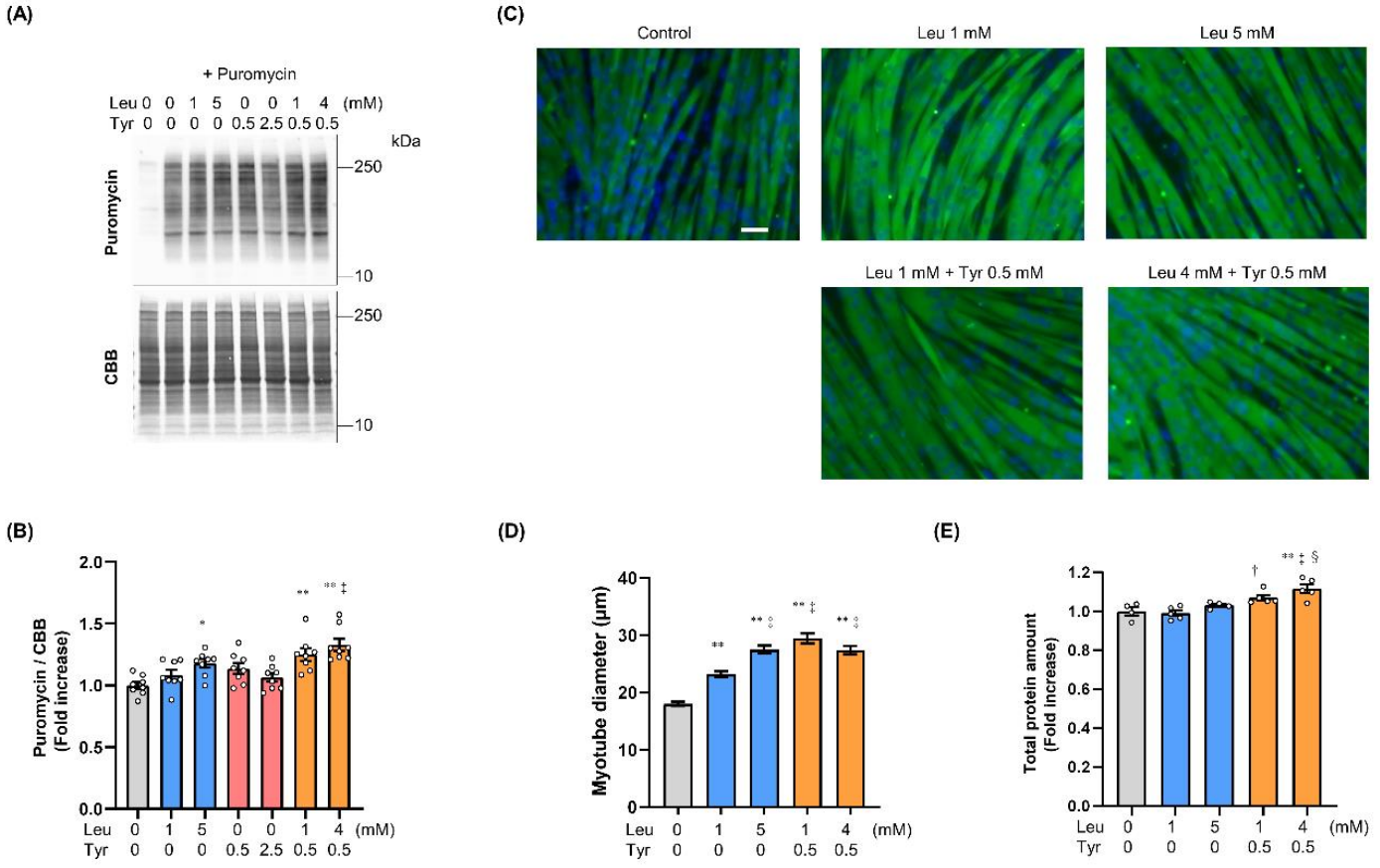

Figure 2. Tyrosine enhances leucine-induced muscle protein synthesis and myotube hypertrophy in C2C12 cells.

Muscle protein synthesis was assessed through the surface sensing of translation (SUnSET) method. (A) Representative images of puromycin incorporation in myoblasts on day 1 post-differentiation as detected

through western blotting and CBB staining. (B) The rate of puromycin incorporation was normalized to the corresponding CBB staining (n = 8). Differentiating C2C12 myoblasts were continuously treated with Leu and/or Tyr during differentiation. (C) Representative images of myotubes stained with MHC (green) and DAPI (blue) on day 5 post-differentiation (scale bar: 50 μm) (D) and myotube diameters (n = 133–142). (E) Total protein levels were evaluated through the BCA analysis on day 5 post-differentiation (n = 4–5). All data represent the fold change with respect to the control (0 mM Leu and 0 mM Tyr). Data are presented as mean ± SEM. Circles represent individual values. * $p < 0.05$, ** $p < 0.01$ vs. control. † $p < 0.05$, ‡ $p < 0.01$ vs. 1 mM Leu. § $p < 0.05$ vs. 5 mM Leu as determined by one-way ANOVA.

4-3-2. Tyr Enhanced Leu-induced Muscle Anabolic Signaling in Isolated Muscles and Muscles of Orally Treated Mice

To determine whether the booster effect of Tyr on Leu could be observed ex vivo at physiological concentrations, we incubated isolated mouse soleus and EDL muscles with the KRB buffer supplemented with Leu and/or Tyr and then measured S6K and 4E-BP phosphorylation levels. The effect of the Leu and Tyr combination on S6K phosphorylation was similar to that induced by 3 mM Leu in both the soleus and EDL muscles (Figure 3A,B). Of note, the 1 mM Leu + 0.5 mM Tyr combination significantly promoted S6K phosphorylation in the soleus muscle as compared to 1 mM Leu (Figure 3A). In both cases, the extent of S6K phosphorylation induced by 0.5 mM and 1 mM Tyr in combination with 1 mM Leu was similar, with no dose dependence observed. 4E-BP phosphorylation showed the same trend as S6K phosphorylation, but to a lesser extent (Figure 3C,D).

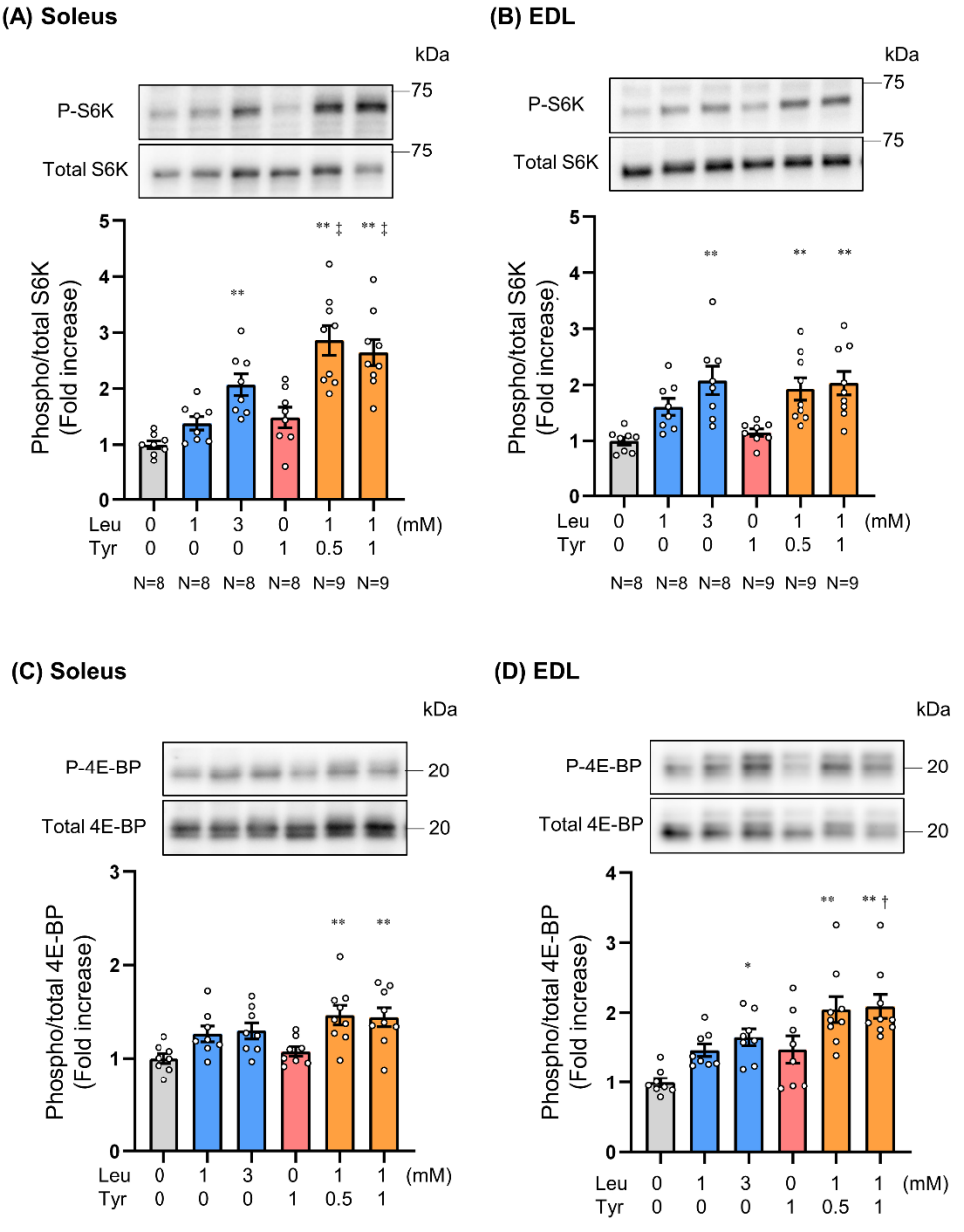

Figure 3. Effect of leucine and tyrosine on S6K and 4E-BP phosphorylation in isolated muscles. Overnight-fasted male C57BL/6J mice were sacrificed, and their soleus and extensor digitorum longus

(EDL) muscles were isolated and incubated in Krebs Ringer Bicarbonate (KRB) buffer containing 0–3 mM Leu and/or 0–1 mM Tyr for 20 min. (A,B) S6K phosphorylation (Thr389) levels in the soleus and EDL muscles. (C,D) 4E-BP phosphorylation (Thr37/46) levels in the soleus and EDL muscles. All data represent the fold change with respect to the control (0 mM Leu and 0 mM Tyr). Data are presented as mean ± SEM (n = 8–9). Circles represent individual values. * $p < 0.05$, ** $p < 0.01$ vs. control. † $p < 0.05$, ‡ $p < 0.01$ vs. 1 mM Leu as determined by one-way ANOVA.

Next, we evaluated the effect of oral Leu administration in combination with Tyr on S6K phosphorylation in the muscles. First, we determined the maximum dose of Leu employed in previous studies, and this was equivalent to the daily intake dose (46,47). To ensure appropriate dosing, amino acids were dispersed in a 10% lipid emulsion and then administered to mice. Thirty minutes after amino acid administration, S6K phosphorylation in the soleus muscle was significantly higher in the Leu- (at a Leu dose of 10 mmol/kg BW) and Leu + Tyr-treated groups (both at doses of 5 mmol/kg BW Leu + 1 mmol/kg BW Tyr and 5 mmol/kg BW Leu + 5 mmol/kg BW Tyr) than in the control group (Figure 4A). S6K phosphorylation in the gastrocnemius muscle was significantly higher in the 10 mmol/kg BW Leu-treated groups and in the 5 mmol/kg BW Leu + 5 mmol/kg BW Tyr-treated groups than in the control group (Figure 4B). In addition, we preliminarily confirmed that S6K phosphorylation levels remained unchanged 15 and 60 min after amino acid administration (data not shown). Serum Leu and Tyr concentrations increased in a dose-dependent manner 30 min after oral amino acid administration (Figure 4C,D). Unexpectedly, serum Tyr concentrations in the 5 mmol/kg BW Leu + 5 mmol/kg BW Tyr-treated groups were significantly higher than those in the 5 mmol/kg BW Tyr-treated groups (Figure 4D). The serum Tyr concentration was lower

than that of Leu even when equal molar amounts of both amino acids were administered (Figure 4C,D). Although the oral bioavailability of Tyr was lower than that of Leu, probably due to its low water solubility, serum Tyr concentrations were positively correlated with S6K phosphorylation in both the soleus and gastrocnemius muscles in the Leu + Tyr-treated groups (Figure 4E–H); this was not the case with Leu.

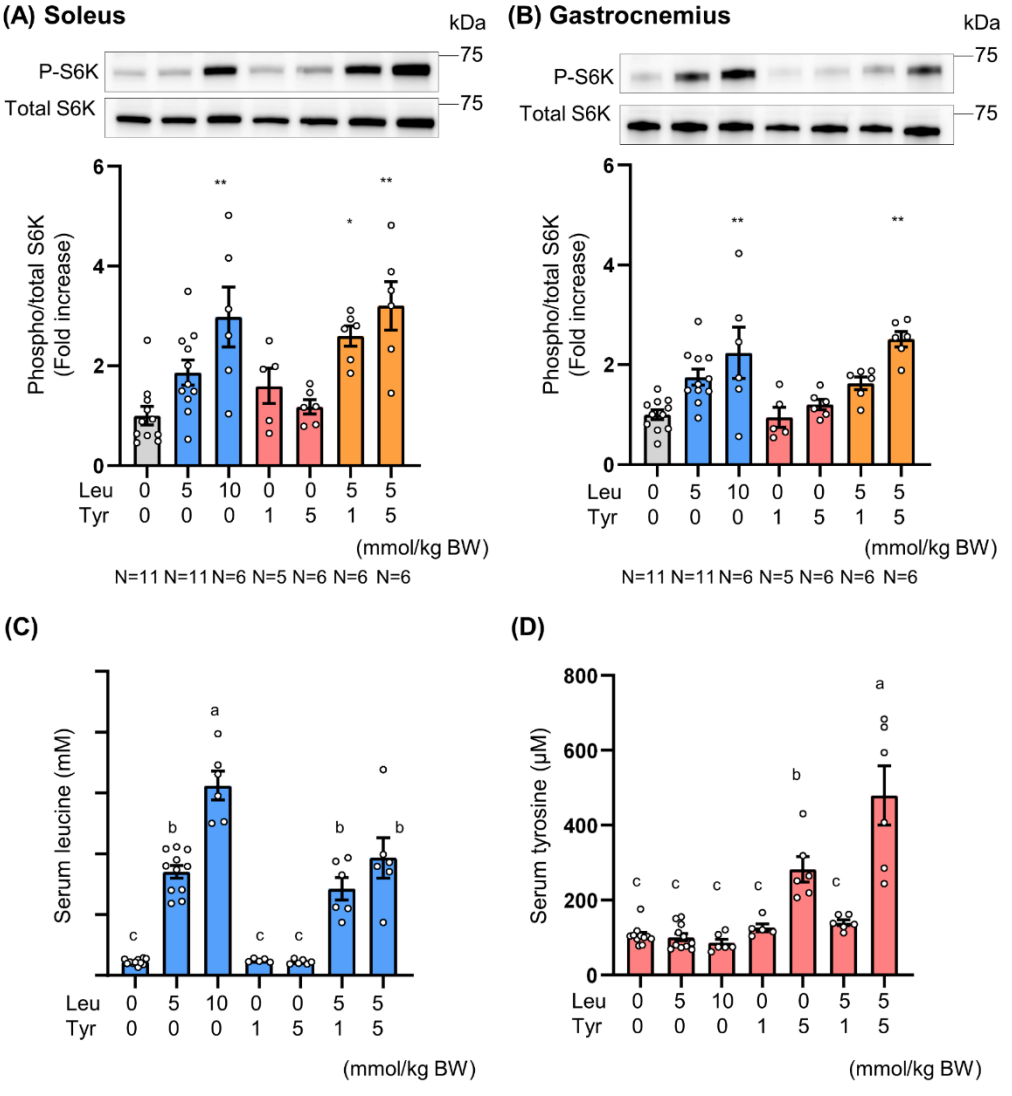

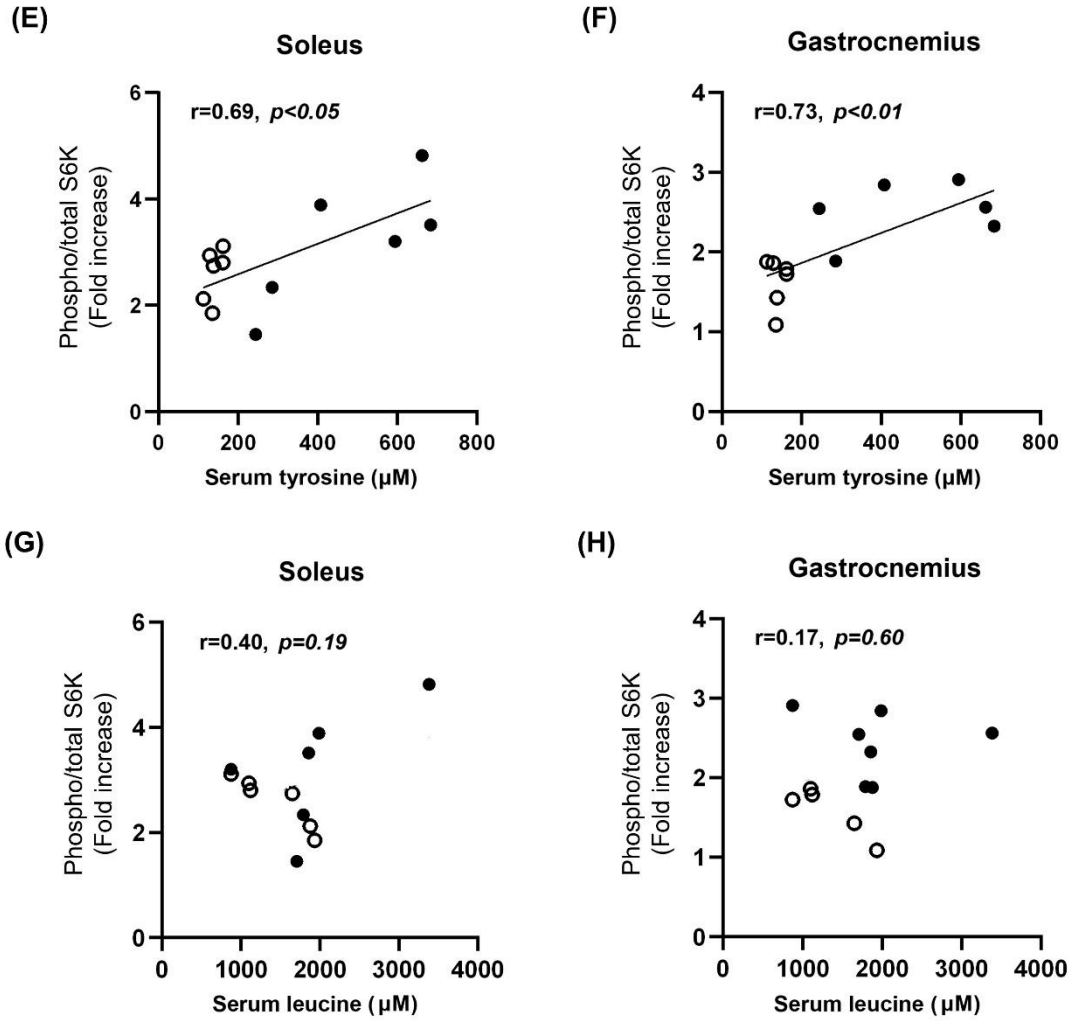

Figure 4. Effect of oral leucine and tyrosine administration on S6K phosphorylation in mice.

A lipid emulsion containing Leu and/or Tyr was intragastrically administered to overnight-fasted mice under isoflurane anesthesia. Muscle and blood samples were collected after 30 min. S6K phosphorylation (Thr389) in the soleus (A) and gastrocnemius (B) muscles was detected by western blotting. Serum leucine

(C) and tyrosine (D) levels were determined through LC-MS/MS. (E–H) The correlation between S6K phosphorylation level and serum tyrosine or leucine concentration in the Leu + Tyr-treated groups is shown. Empty circles with a black outline and black circles indicate the 5 mmol/kg BW Leu + 1 mmol/kg BW Tyr and 5 mmol/kg BW Leu + 5 mmol/kg BW Tyr treatments, respectively. All data represent the fold change with respect to the control (0 mmol/kg BW Leu + 0 mmol/kg BW Tyr). Data are presented as mean ± SEM (n = 5–11). Circles represent individual values. ** $p < 0.01$ vs. control as determined by one-way ANOVA (A,B). Different letters (a–c) represent significant differences ($p < 0.05$) as determined by one-way ANOVA (C,D). A correlation analysis was performed using Pearson's correlation coefficient (E–H).

4-3-3. Molecular Mechanism by Which Tyr Enhances Leu-Induced S6K Phosphorylation

To provide mechanistic insights into the booster effect of Tyr on Leu, first, we hypothesized that the incorporation of Leu into muscle cells is enhanced in presence of Tyr, and then we measured free Leu and Tyr levels in treated C2C12 cells and isolated muscles. However, we found that although Tyr was more significantly incorporated into cells than Leu at the same exposure concentrations, Leu incorporation remained unchanged irrespective of Tyr administration (Figure S2).

Recent studies have shown that Sestrin1 and 2 bind to Leu and are involved in Leu-induced activation of mTORC1 signaling (37,41). We compared the protein expression levels of Sestrin1 and 2 between C2C12 myoblasts, EDL muscles, gastrocnemius muscles, and soleus muscles. Both Sestrin1 and Sestrin2 were more highly expressed in C2C12 cells and soleus muscles than in EDL and gastrocnemius muscles (Figure 5A). Following the suppression of Sestrin1 expression in C2C12 cells through siRNA transfection, Sestrin2 expression was upregulated; however, following the suppression of Sestrin2 expression, Sestrin1

expression slightly decreased (Figure 5B). Thus, we examined S6K phosphorylation in C2C12 cells treated with Leu and/or Tyr under both Sestrin1 and 2 suppression. As Sestrin1 and 2 inhibit mTORC1 by interacting with GATOR2, we expected that the suppression of the expression of these proteins would increase the basal S6K phosphorylation state and attenuate Leu-induced S6K phosphorylation. However, both the basal and Leu-induced S6K phosphorylation levels remained unchanged following the suppression of the expression of these proteins; S6K phosphorylation was found to be promoted by treatment with Tyr and was further enhanced following treatment with Leu in combination with Tyr (Figure 5C). Leucyl-tRNA synthetase (LRS) has been proposed as an intracellular Leu sensor that induces mTORC1 activation (51). However, Leu- and/or Tyr-induced S6K phosphorylation remained unchanged following LRS knockdown (Figure S3).

Figure 5. Involvement of Sestrin1 and 2 in leucine and tyrosine-induced S6K phosphorylation.

(A) Sestrin1 and 2 expression in mouse C2C12 myoblasts, EDL muscles, gastrocnemius muscles, and soleus muscles was determined through western blotting. (B) Sestrin1 and 2 mRNA expression levels in C2C12 myoblasts subjected to siRNA transfection, on day 1 post differentiation, were determined via qRT-PCR (n = 3). (C) S6K phosphorylation (Thr389) in C2C12 myoblasts on day 1 post differentiation in response to 15 min of stimulation with Leu and/or Tyr following the downregulation of Sestrin1 and 2 expression using siRNA (n = 6). All data represent the fold change compared with the scramble Ctrl (Scr) siRNA (0 mM Leu and 0 mM Tyr). Data are presented as mean ± SEM. Circles represent individual values. * $p < 0.05$, ** $p < 0.01$ vs. Ctrl (Scr siRNA). † $p < 0.05$ vs. 0.5 mM Tyr (Scr siRNA). ‡ $p < 0.01$ vs. 1 mM Leu + 0.5 mM Tyr (Scr siRNA). § $p < 0.01$ vs. Ctrl (Sestrin1, 2 siRNA) as determined by two-way ANOVA.

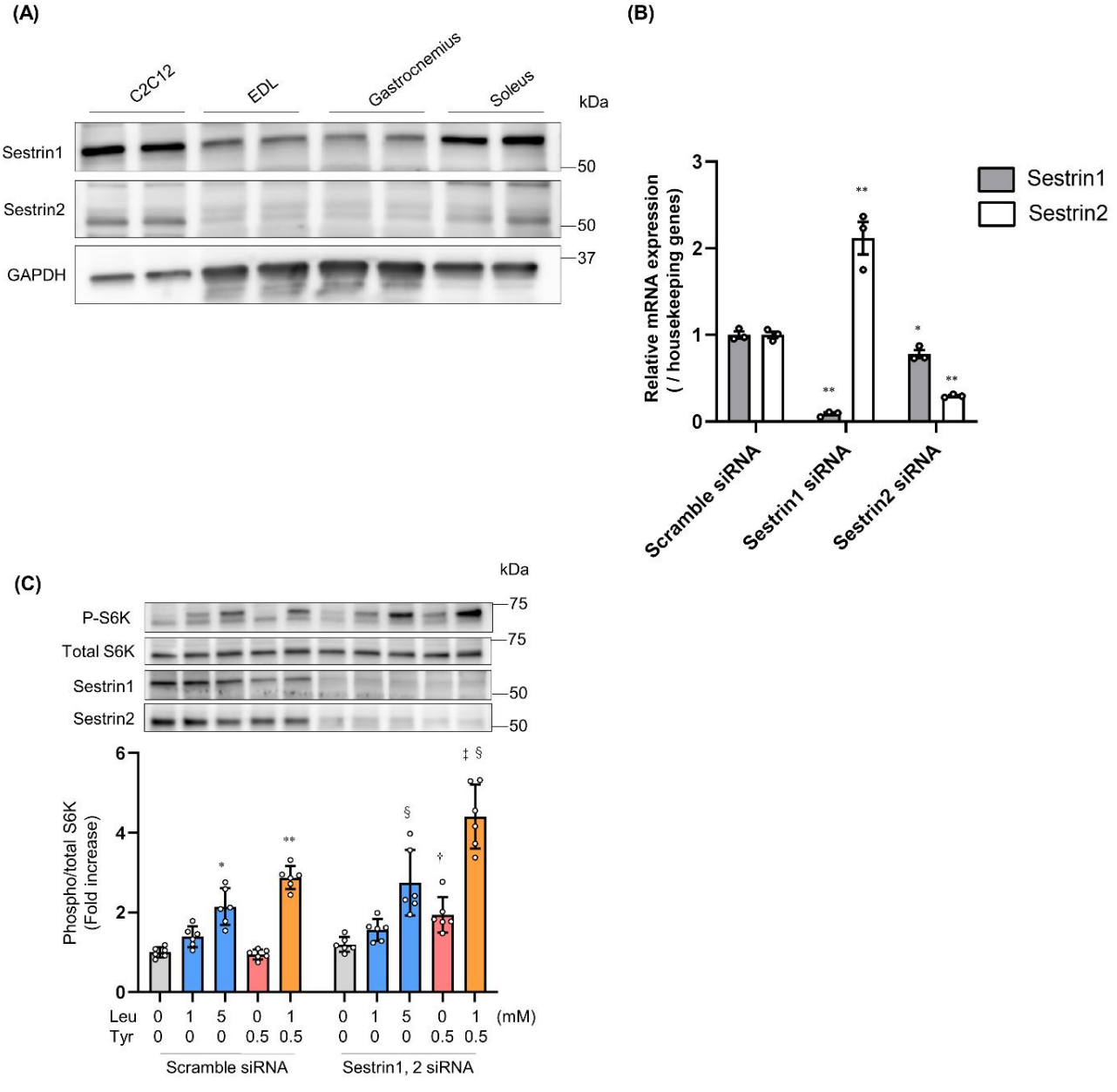
(A)
C2C12
EDL
Gastrocnemius
Soleus
kDa
Sestrin1
Sestrin2
GAPDH
50
50
37
(B)
Relative mRNA expression
(/ housekeeping genes)
Sestrin1
Sestrin2
Scramble siRNA
Sestrin1 siRNA
Sestrin2 siRNA
(C)
kDa
P-S6K
Total S6K
Sestrin1
Sestrin2
75
75
50
50
Phospho/total S6K
(Fold increase)
Leu
Tyr
(mM)
Scramble siRNA
Sestrin1, 2 siRNA

CHAPTER 4-4. DISCUSSION

In this experiment, we demonstrated that Tyr enhances Leu-induced mTORC1 signaling activation. This phenomenon was confirmed through both in vitro and in vivo experiments. To the best of our knowledge, this is the first study to elucidate the contribution of Tyr to mTORC1 signaling.

Leu is unique an amino acid among EAA in that it stimulates anabolic signaling in muscles through the phosphorylation of mTOR, 4E-BP, and S6K (30). The findings of previous in vitro studies on C2C12 cells have suggested that the Leu concentration threshold is approximately 5 mM, and that above this threshold, it induces significant levels of S6K phosphorylation, which is necessary for increased protein synthesis in myotubes (52,53). However, as only plasma Leu concentrations of approximately 1.5 mM have been observed in human subjects after the ingestion of high Leu doses (approximately 9 g) (54), a Leu concentration of 5 mM is assumed to be beyond physiological concentrations. The transient anabolic response induced by treatment with 1 mM Leu + 0.5 mM Tyr, which falls within the upper physiological concentration range, was equivalent to or greater than that induced by 5 mM Leu (Figure 1E–I). Our data indicated that the combination of Leu and Tyr at the appropriate ratio lowers the threshold for Leu-induced S6K phosphorylation to a level that falls within the physiological concentration range. The slope of the dose–response curves for Leu concentration versus phosphor-S6K increased with Tyr concentration, which also supported this change in threshold (Figure 1C). Continuous Leu supplementation during differentiation increased myotube diameter but did not affect total protein levels (Figure 2D,E). Our findings are consistent with those of previous studies that showed that Leu preferentially induces myofibrillar protein synthesis (53,55). In contrast, continuous supplementation with Leu and Tyr significantly increased both myotube diameter and total protein levels. Since it has been postulated that myofibrillar proteins are more responsive

to amino acids compared to cytoplasmic proteins (56), the combination of Leu and Tyr may increase both myofibrillar protein and cytoplasmic protein levels, which in turn increased total protein levels in myotubes.

The booster effect of Tyr on Leu-induced activation of anabolic signaling was also confirmed in isolated muscles. The extent of S6K and 4E-BP phosphorylation induced by the 1 mM Leu + 0.5 mM Tyr treatment was found to be equal to or greater than that induced by the 3 mM Leu treatment, especially in the soleus muscle (Figure 3). The intensity of the effect observed after incubation with 3 mM Leu was equivalent to that observed in mice with serum concentrations resulting from the ingestion of the maximum Leu dose of 10 mmol/kg BW (Figure 4C). In addition, S6K and 4E-BP phosphorylation seemed to be highest at Tyr concentrations of 0.5 mM and 1 mM, respectively, in combination with 1 mM Leu. Measurement of free Leu and Tyr intracellular levels showed that Tyr is more readily taken up by muscle cells than Leu (Figure S2), suggesting that high Tyr concentrations may not contribute in further promoting the anabolic signaling response. Our findings suggested that the delivery of Leu and Tyr to muscles at the appropriate ratio is important for inducing this booster effect, and that blood Leu and Tyr concentrations of 1 and 0.5 mM, respectively, may be optimal.

Thirty minutes after oral administration of 5 mmol/ kg BW Leu + 5 mmol/ kg BW Tyr, serum Leu and Tyr concentrations reached approximately 1.5 and 0.5 mM, respectively, and induced significant S6K phosphorylation in both the soleus and gastrocnemius muscles (Figure 4A,B). Serum Tyr concentrations following the oral administration of equal Tyr doses significantly increased upon the co-administration of Leu and Tyr (Figure 4D). However, further investigation is required to determine whether the simultaneous presence of Leu and Tyr in the intestinal tract can truly affect Tyr absorption. Although there was a variation in serum Tyr levels, probably due to its low water solubility and low bioavailability, these levels were

positively correlated with S6K phosphorylation levels (Figure 4E,F). Our data suggest that postprandial blood Tyr concentration is in an appropriate ratio with that of Leu, a key determinant of muscle anabolic signaling.

Notably, we found that the inhibition of Sestrin1 and 2 expression did not affect the Leu-induced S6K phosphorylation (Figure 5C); however, it is possible that the knockdown level was insufficient, and the results could have been different if the extent of knockdown (or knockout) had been greater. As multiple intracellular Leu sensors, such as LRS, SAR1B, and perhaps other unknown factors, have been identified or proposed (51,57–59), their expression may be upregulated in a compensatory manner, and this might maintain Leu-induced S6K phosphorylation under Sestrin1 and 2 suppression. The inhibition of LRS expression did not affect Leu- and/or Tyr-induced S6K phosphorylation (Figure S3). LRS has been identified in HEK293 cells (51); however, inhibition of its expression in C2C12 cells suppressed muscle differentiation but did not affect muscle hypertrophy (60). These findings suggest that LRS contribute little to the regulation of mTORC1 activity in skeletal muscles. Another Leu sensor, SAR1B, is highly expressed in skeletal muscles (57). However, the dissociation constant of SAR1B from Leu was lower than that of the Sestrins from Leu in HEK293T cells. SAR1B is thought to respond to low Leu levels to maintain basal mTOR activity. Thus, the functional relationship between Leu sensors and mTORC1 activity in the muscle cells should be explored in future studies. Tyr induced S6K phosphorylation under Sestrin1 and 2 suppression (Figure 5C). In the presence of Leu, the interaction between Sestrins and GATOR2 is disrupted through the binding of Leu to Sestrins (37,41). Leu-dependent Sestrin divergence conditions are analogous to the state of inhibition of Sestrin expression, and in this state, Tyr can activate mTORC1 via an unknown interaction with GATOR2. As Phe also exerted a booster effect on Leu-induced S6K phosphorylation

(Figure 1A,B), the structural features of both Tyr and Phe are probably involved in the molecular mechanism; however, the precise mechanism by which Tyr (and Phe) promotes mTORC1 activation in the presence of Leu is yet to be elucidated.

We found the protein expression levels of Sestrin1 and 2 in the soleus muscle to be higher than that in the EDL and gastrocnemius muscles (Figure 5A); this might explain the more significant booster effect of Tyr on Leu-induced mTORC1 activation in the soleus muscle (Figures 3 and 4). However, this speculation is inconsistent with in vitro findings, as the booster effect of Tyr on Leu was found to be significant under Sestrin1 and 2 suppression (Figure 5C). Recent studies have shown that Sestrin1 levels decrease with lack of use or aging, and that it is a key regulator of anabolic and degradative pathways that pre-vent muscle atrophy (61–63). Sestrin1 is upregulated following acute resistance exercise (64) and downregulated following chronic treadmill exercise (65). Although the relationship between the change in Sestrin expression and mTORC1 activity is not clearly understood, and as changes in the expression of other confounding factors that affect mTORC1 activity need to also be considered in this regard, the expression levels of Sestrins could partially explain the upregulation in Leu (and Tyr)-induced mTORC1 activation with increased MPS following resistance exercise- or age-related anabolic resistance.

It should be noted that this study has some limitations. First, in our in vivo experiments, we only evaluated S6K phosphorylation and did not evaluate the actual rate of MPS. Second, the acute anabolic response level, including S6K phosphorylation and MPS rate, is not sufficient to estimate the divergence of chronic intervention-induced changes in muscle hypertrophy (66). Although we demonstrated that Tyr serves as a booster to enhance Leu-induced MPS and muscular hypertrophy in vitro (Figure 2), further

studies are needed to determine whether long-term nutritional intervention with Leu and Tyr, or a protein source that contains them at high levels, could result in muscular hypertrophy in vivo.

CHAPTER 5. EXPERIMENT #2

TRPM8-mediated cutaneous stimulation modulates motor neuron activity during treadmill stepping in mice

CHAPTER 5-1. INTRODUCTION

Motor neurons (MNs) are generally recruited from the smallest to the largest with an increasing load following the size principle (67). MNs recruited at a low force tend to constitute small motor units (MUs), while large MNs are recruited when higher forces are needed, and they constitute the large MUs (68). However, there are some exceptions (69), for example, the order of MU recruitment can be changed by electrically stimulating the cutaneous afferents. The afferent stimulation generates inhibitory responses in the small MUs and excitatory responses in the large MUs (70–72). These findings suggest that cutaneous afferent input modulates MN excitability via somatosensory reflex pathways. Cutaneous stimulation has the potential to induce adaptive plasticity in the muscles (73) and is applied for the treatment of various neurological and musculoskeletal disorders (74,75).

Skin cooling (SC) induced by a cold environment has been reported to enhance electrical activity in muscle during repetitive exercise without changes in muscle temperature (76). SC at 25 °C during a slow ramp contraction also changes the MU recruitment pattern and selectively induces large MU recruitment (77). Furthermore, in practical rehabilitation trials, recent studies have shown that maintaining the skin temperature at around 25 °C, using a gel-cooling pad on the quadriceps muscle, enhances muscle activity at 15% maximum voluntary contraction (78) and improves the rate of force development in the early phase

of contraction (79). Based on these studies, it is presumed that maintaining the skin temperature at 25 °C is appropriate for modulating MN excitability without a reduction in the muscle temperature.

Transient receptor potential (TRP) channels play critical roles in the transduction of temperature and a sub-family of M8 (TRPM8) is activated at a temperature of ≤ 25-28 °C (80). It has been assumed that activation of TRPM8, expressed in the peripheral nerves, is responsible for SC-induced cutaneous input. TRPM8 is also activated by chemical agents, such as menthol and icilin (81–83). We have previously shown that the application of menthol gel on the skin over working muscles enhances muscle activity at a low load (35% maximum voluntary contraction) in both adult and elderly individuals (84). These findings suggest that TRPM8-mediated sensory input may be responsible for SC-mediated MN excitability. In addition, because the application of menthol gel neither requires any extensive equipment for SC nor limits any movement for subjects, this strategy might be useful to train elderly individuals to recruit large MUs at low-load exercise and to prevent age-related loss of type 2 muscle fibers (3,7).

However, our previous study assessing MU recruitment with surface electromyography could only indicate the activity of the outer layer of the muscle. Thus, it remains unclear whether TRPM8-mediated cutaneous input in the working muscle modulates spinal MN excitability and induces large MU recruitment. The early response gene c-fos has been used in identifying activated neurons in the brain and spinal cord while performing various tasks (85,86). Previous studies have demonstrated that the number of MNs expressing c-fos increases after a single bout of treadmill stepping in a time- and intensity-dependent manner (87–89). Detection of c-fos is considered a marker of neural activity in the spinal cord. The purpose of this study was to investigate the effects of TRPM8-mediated cutaneous stimulation combined with exercise on the modulation of spinal MN excitability. In this experiment, by using c-fos immunostaining,

we found that topical application of a TRPM8 agonist with low-load treadmill stepping promoted c-fos expression in the large MNs, which were supposed to be the fast MNs innervating the type 2 fibers and constitute the large MUs.

CHAPTER 5-2. MATERIALS AND METHODS

5-2-1. Animals

Male C57BL/6J mice (9−14 week-old) were purchased from CLEA Japan (Tokyo, Japan) and maintained under a controlled condition (temperature, 23 ± 2 °C; humidity, 55 ± 10%; and lighting, 07:00 to 19:00 h). The mice were provided with standard chow (CE-2; CLEA Japan, Tokyo, Japan) and water ad libitum. All animal experiments were conducted at the Experimental Animal Facility of the Kao Corporation's R&D Department. The study was approved by the Kao's Animal Care Committee, and all experiments followed the guidelines of the committee.

5-2-2. Animal Experiment 1

After acclimatization, the mice (n = 6) were anesthetized with isoflurane (Abbott Japan, Tokyo, Japan), and the hairs of the hindlimbs were shaved by animal clippers. Icilin (QJ-5946, Combi-Blocks, San Diego, CA, USA) was dissolved in 80% DMSO (Wako, Osaka, Japan) and 20% PBS solution, and the concentration was adjusted to 1.5% (w/v). Approximately 100 μL of the icilin solution was applied on the right hindlimb, whereas a control solution (80% DMSO, 20% PBS) was applied on the left hindlimb of each mouse under isoflurane anesthesia. The solution was gently applied to all parts of the hindlimb thrice with a cotton swab. To provide adequate time for c-fos expression, the mice were returned to their cages and were perfused 90 min after the application.

5-2-3. Animal Experiment 2

A 10-lane motorized rodent treadmill (MK-680; Muromachi Kikai, Tokyo, Japan) with no incline was used for treadmill stepping. The experiment was conducted with three days of sessions. After shaving the hairs from the hindlimbs, all mice were accustomed to treadmill stepping at a speed of 10 m/min for 30 min

for the initial two days. On the last day, the mice (n = 55) were randomly divided into five groups: Sedentary (Sed, n = 9), Sedentary+icilin (Sed+icilin, n = 10), Low-speed stepping (Low-speed stp, n = 12), High-speed stepping (High-speed stp, n = 12), and Low-speed stepping+icilin (Low-speed stp+icilin, n = 12). The mice were topically administrated with icilin solution or control solution on all parts of the hindlimbs as noted in **5-2-2**, followed by conducting treadmill stepping or home cage activity. The treadmill stepping was conducted according to the following program: low-speed, 12 m/min for 60 min; and high-speed, 18−20 m/min for 60 min to detect activated neurons as previously described (88). The stepping speed was set to increase by 2 m/min up to each maximal speed. The mice were returned to their cages and were perfused 60 min after the treadmill-stepping bout. All mice were kept fasting for 3 h before the treadmill stepping.

5-2-4. Tissue collection

The mice were anesthetized with isoflurane and perfused transcardially with 20−30 mL of PBS supplemented with 1 unit/mL of heparin sodium (Mochida Pharmaceutical, Tokyo, Japan), followed by 20−30 mL of 4% paraformaldehyde phosphate buffer solution (4% PFA; Wako, Osaka, Japan). The vertebral column containing the spinal cord was dissected and post-fixed in 4% PFA overnight at 4 °C. The spinal cords were carefully dissected from the vertebral column and impregnated with 30% sucrose in PBS for over 3 days at 4 °C. With the dorsal root ganglion of L5 as a landmark, the lower lumbar segments (L3−L5) were embedded in OCT compound (Sakura Finetek Japan, Tokyo, Japan) and stored at − 80 °C.

5-2-5. Immunohistochemistry

The frozen spinal cord blocks were transversely sectioned to 30 μm thickness by a cryostat. For each mouse, approximately 100−120 of the sections were sampled from the L3−L5 segment and collected in 12

consecutive groups of 10 free-floating sections in PBS with sodium azide (Rockland Immunochemicals, Limerick, PA, USA). Approximately 24 sections per mouse, 2 out of 10 sections randomly picked up from each group, were used for immunolabeling in a free-floating manner. The sections were washed in 0.1 M PB and incubated in primary antibodies against c-fos (rabbit, 1:5000, #226 003, Synaptic Systems, Goettingen, Germany) and choline acetyltransferase (ChAT, goat, 1:200, AB144P, EDM Millipore, Temecula, CA, USA) with a diluted solution (1% normal donkey serum, 0.3% TritonX-100, 0.25% λ-carrageenan, 0.01% NaN_3 in PBS) on a shaker at 4 °C for three days. The sections were washed in PBS with 0.3% TritonX-100 (PBS-T) thrice and incubated with secondary antibodies (Alexa 488-conjugated donkey anti-rabbit and Alexa 568-conjugated donkey anti-goat (1:1000, Molecular Probes, Thermo Fisher Scientific, Pittsburg, PA, USA)) with the diluted solution on a shaker for 1 h at room temperature. The sections were then washed in PBS thrice and mounted on Micro Slide Grass (Matsunami Grass, Osaka, Japan). Coverslips were placed with VECTASHIELD Hard-Set Mounting Medium (Vector Labs, Burlingame, CA, USA).

5-2-6. Analysis of the activated neurons

Digital images were acquired with an all-in-one fluorescence microscope (BZ-X700, Keyence, Osaka, Japan). All images were obtained at a magnification of 10×. For quantitative analysis, BZ Analyzer (Keyence) was used to count the c-fos positive neurons by manual tagging and to measure the soma size of ChAT labeling MN. A ChAT-positive cell merged with c-fos in lamina IX was defined as a c-fos$^+$ MN. ChAT-positive cells located in the range of 400 μm width and 300 μm length centering on the central canal were defined as cholinergic interneurons (INs) near the central canal (89) about previous studies of mouse lumbar spinal cord (90,91), and the number of these cells merged with c-fos was counted. Since

immunostaining images of some mice were not quantifiable probably due to inadequate perfusion and fixation, some samples were excluded from the analysis. The numbers of mice in the Sed, Sed+icilin, Low-speed Stp, High-speed Stp, and Low-speed Stp+icilin groups included in the analysis were 9, 9, 11, 12, and 11 respectively. The quantification was blindly performed by assigning a code number to each mouse and opening the code after all quantification was completed.

5-2-7. Statistical analysis

All data are represented by the mean ± S.D. Group differences between the two groups were tested with unpaired Student's t-tests. Moreover, group differences among > 3 groups were tested with one-way ANOVA followed by Tukey's post hoc test. Comparison of the soma sizes was performed by two-way ANOVA followed by Tukey's post hoc test. Correlation was assessed by Pearson's correlation coefficient. The threshold of significance was set at $p<0.05$. All analysis was performed using Prism 6 statistical software (GraphPad Software, San Diego, CA, USA).

CHAPTER 5-3. RESULTS

5-3-1. Peripheral stimulation with a TRPM8 agonist induces c-fos expression in the spinal cord dorsal horn

To confirm whether TRPM8-mediated SC stimulation is induced by the cutaneous afferents, we examined the expression of c-fos in the mouse spinal cord dorsal horn following application of a specific TRPM8 agonist, icilin (82) on the hindlimbs. We compared the levels of icilin-evoked c-fos expression to those evoked by the control solvent in lamina I and II of the dorsal horn, as described previously (92). Application of 1.5% icilin induced significant numbers of c-fos positive nuclei in the ipsilateral dorsal horn as compared to the contralateral side (Figure 6). We preliminary confirmed that 1.5% icilin was enough to induce the c-fos expression in the spinal cord dorsal horn, because the levels were similar to those of 3% icilin, a maximum dissolved concentration (data not shown). Thus, we used 1.5% icilin in the following experiment.

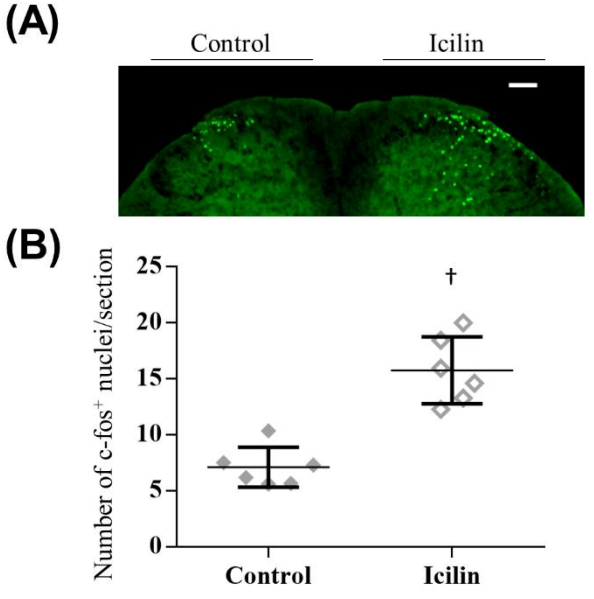

Figure 6. Icilin induced c-fos expression in lamina I and II of the spinal cord dorsal horn.

Representative image of the spinal dorsal horn is shown (A). Topical application of icilin leads to increased levels of c-fos protein in the L3–L5 region of the ipsilateral dorsal horn (Icilin) as compared to that in the contralateral side (Control) (B). Each symbol represents an individual mouse. The horizontal lines indicate the mean values. Scale bar = 100 μm. Compared with the control, †$p<0.01$. Data are represented as the means ± S.D.

5-3-2. TRPM8-mediated cutaneous stimulation modulates c-fos positive MNs following treadmill stepping

To evaluate the effects of topical application of icilin with treadmill stepping on the activation of MNs, we defined ChAT-labeled neurons in lamina IX as MNs and observed the c-fos$^+$ MNs in the sections of spinal cord ventral horn (Figure 7). In the quantitative evaluation of c-fos$^+$ MNs, the number of c-fos$^+$ MNs per section was increased by treadmill stepping, whereas there was no difference in the icilin stimulation or increased stepping speed (Figure 8A). As the number of c-fos$^+$ MNs was unchanged among the Low-speed stp, High-speed stp, and Low-speed stp+icilin groups, we next evaluated the soma size of c-fos$^+$ MNs. The soma size distribution of c-fos$^+$ MNs was greatly changed by icilin stimulation or increasing the stepping speed (Figure 8B). The average soma size of the total c-fos$^+$ MNs was also higher in the Low-speed stp+icilin group and showed an increasing trend in the High-speed stp group than that in the Low-speed stp group (Figure 8C). We especially focused on the MNs ≥ 1000μm^2 of soma size because these neurons are fast MNs that innervate type 2 fibers (93,94). Thus, in the present experiment, we defined that MNs of ≥ 1000 μm^2 constitute the large MUs. The percentage of large soma size (≥1000 μm^2) of c-fos$^+$

MNs was also higher in the Low-speed stp+iciln and High-speed stp groups than in the Low-speed stp group (Figure 8D). There were few c-fos$^+$ MNs observed in the Sed and Sed+icilin groups, and thus, we independently showed the size comparison between both groups in Supplemental Figure 4. The average soma size and the percentage of large soma size of c-fos$^+$ MNs were unchanged between the Sed and Sed+icilin groups (Figure S4).

Figure 7. Representative images of activated MNs in the spinal cord ventral horn.

Sections immunostained with c-fos (green) and ChAT (red) are shown for the sedentary, sedentary+icilin, low-speed stepping, high-speed stepping, and low-speed stepping+icilin groups. C-fos merged in the nuclei of ChAT-positive soma in lamina IX indicates activated (c-fos$^+$) MN (white arrowheads). Scale bar = 100 μm.

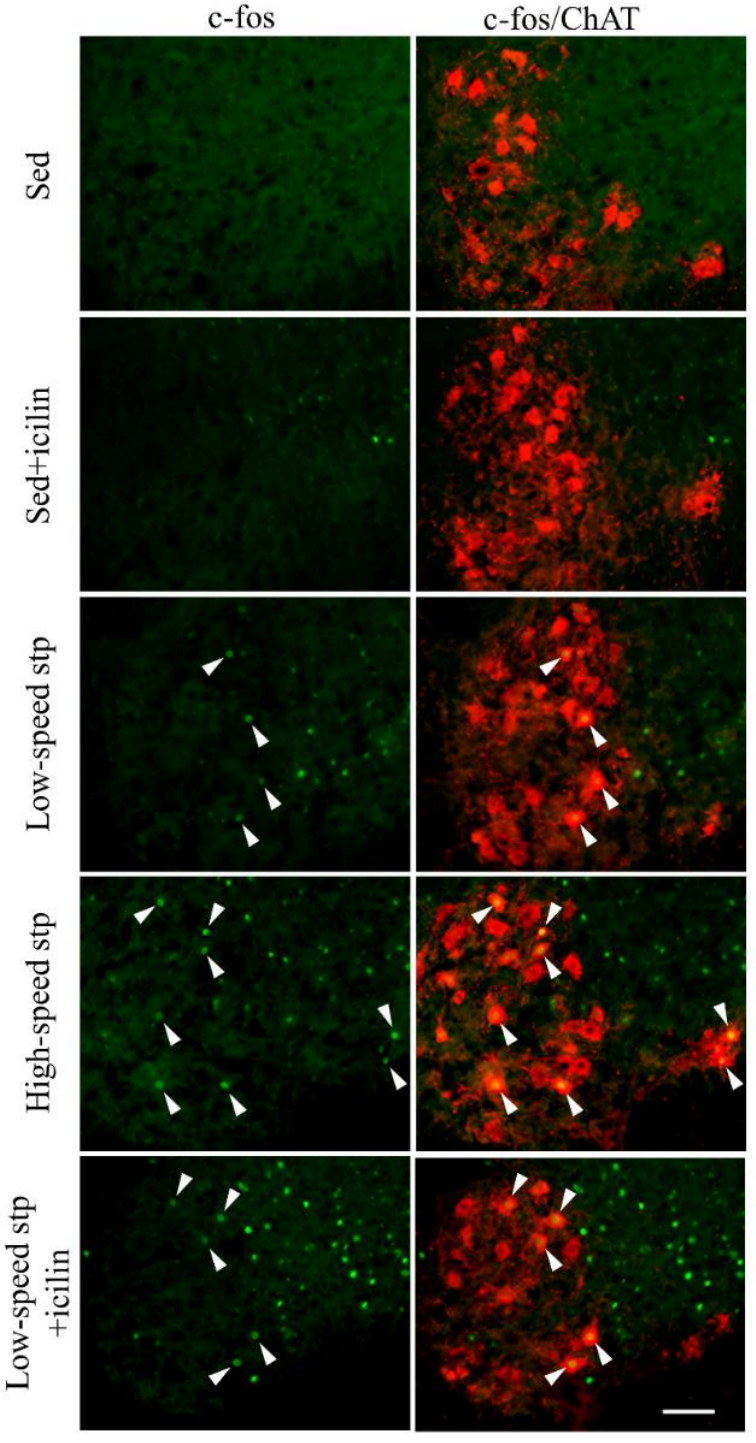
c-fos
c-fos/ChAT
Sed
Sed+icilin
Low-speed stp
High-speed stp
Low-speed stp
+icilin

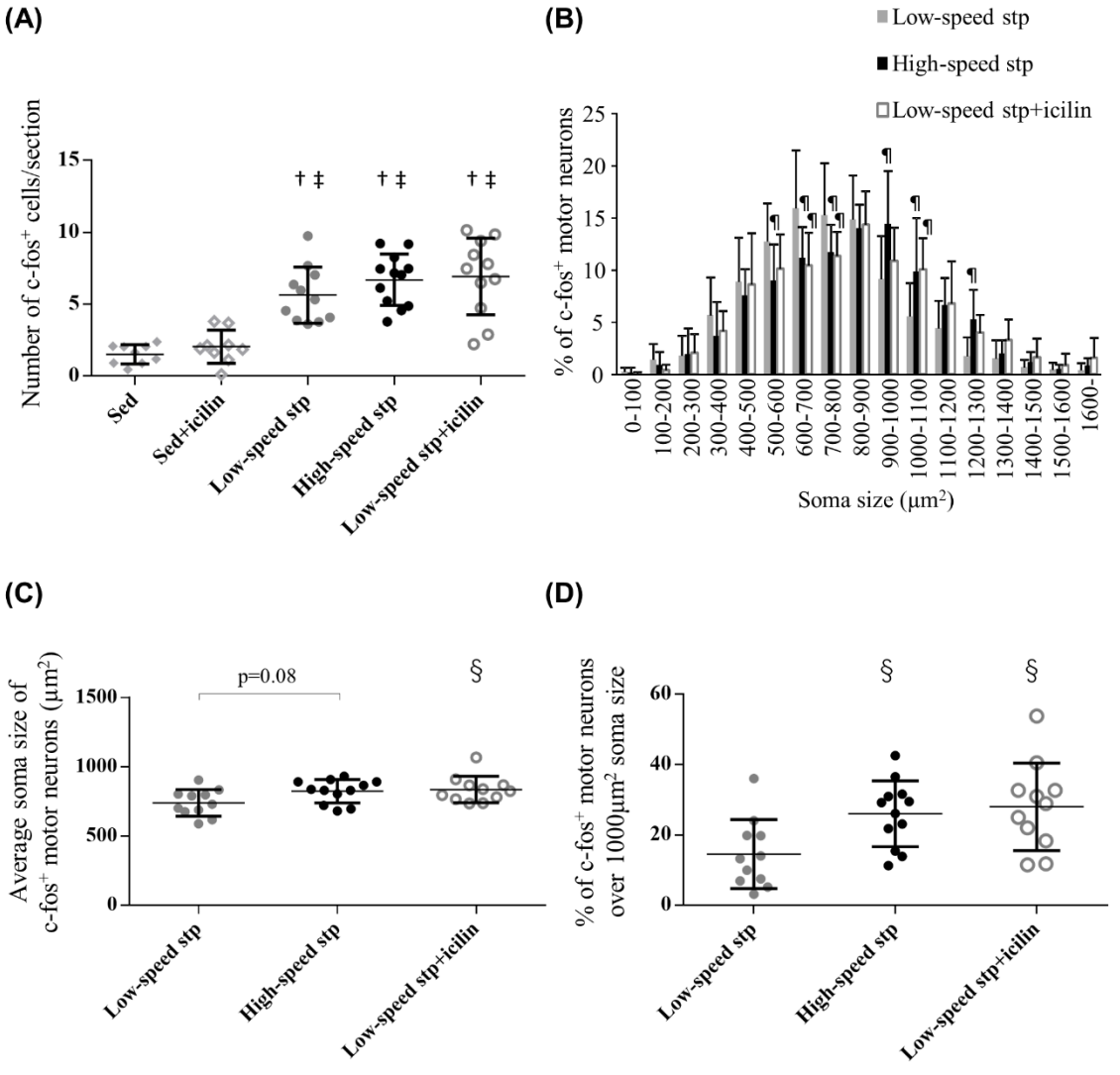

Figure 8. Treadmill stepping with icilin stimulation does not change the number of c-fos+ MNs but modulates the soma size of c-fos$^+$ MNs.

Quantitative results of c-fos$^+$ ChAT-labeled MNs in immunostained images of the spinal cord are shown. The number of c-fos$^+$ MN per section is shown for (A). The distribution of the c-fos$^+$ MNs with respect to their soma sizes (μm^2) is shown for the stepping groups (B). The average soma size of the total c-fos$^+$ MNs and the percentage of large soma size ($\geq 1000\ \mu m^2$) of the c-fos$^+$ MNs are shown in (C) and (D), respectively. Each symbol represents an individual mouse. The horizontal lines indicate the mean values. Compared with Sed group, †$p<0.01$; Compared with Sed+icilin group, ‡$p<0.01$; Compared with Low-speed stp group, §$p<0.05$, ¶$p<0.01$. Data are represented as the means ± S.D.

5-3-3. TRPM8-mediated cutaneous stimulation modulates c-fos positive cholinergic INs following treadmill stepping

Spinal interneurons (INs) relay signals between the sensory neurons and MNs. To reveal mechanistic insights on the modulating MN excitability, we focused on the cholinergic INs, which are likely to be involved in sensory processing and motor output (95,96). We identified cholinergic INs based on their distance from the central canal (Figure 9A) as described previously (89–91). The number of activated cholinergic INs was higher in the three-stepping groups than that in the Sed and Sed+icilin groups (Figure 9B). This was also higher in the Low-speed stp+icilin group and showed an increasing trend in the High-speed stp group than in the Low-speed stp group. Subsequently, we evaluated the correlation between the number of activated cholinergic INs and the percentage of large soma size ($\geq 1000\ \mu m^2$) of the activated MNs in each mouse (Figure 9C). The activation of the cholinergic INs showed a significant positive correlation with the activation of the large MNs.

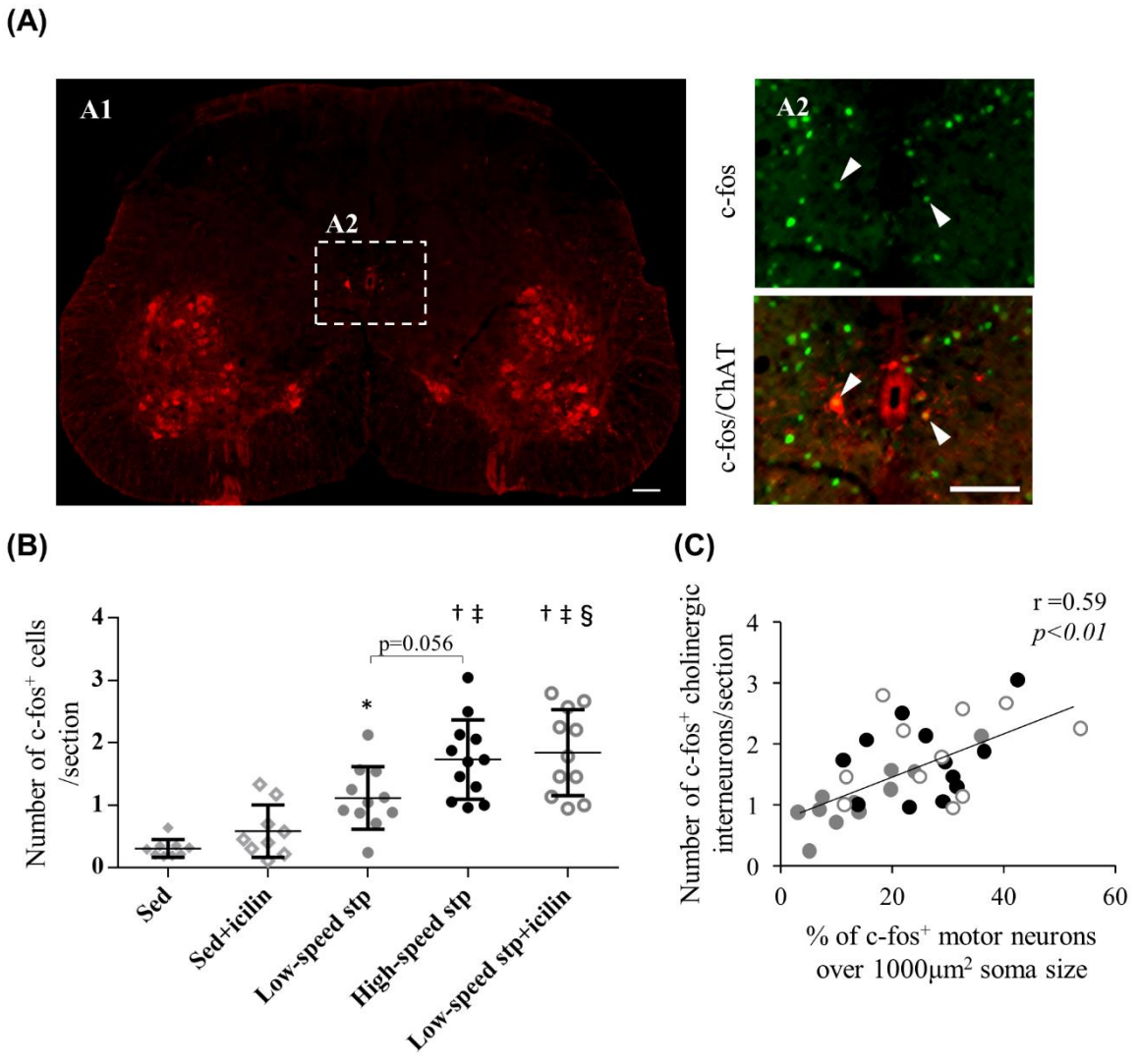

Figure 9. Treadmill stepping with icilin stimulation activates the cholinergic INs.

Cholinergic INs near the central canal were identified in the range of 400 μm width and 300 μm length centering on the central canal (A1). Representative images of the c-fos$^+$ cholinergic INs near the central

canal (white arrowheads) immunostained with c-fos (green) and ChAT (red) are shown (A2; box with white dashed line). Scale bar = 100 μm. The number of c-fos$^+$ cholinergic INs near the central canal per section is shown for the sedentary, sedentary+icilin, low-speed stepping, high-speed stepping, and low-speed stepping+icilin groups (B). Each symbol represents an individual mouse. The horizontal lines indicate the mean values. Compared with Sed group, *$p<0.05$, †$p<0.01$; Compared with Sed+icilin group, ‡$p<0.01$; Compared with Low-speed stp group, §$p<0.05$. Data are represented as the means ± S.D. The correlation between the activation of cholinergic INs and the activation of large MNs in all mice of the three-stepping group (n = 34) is shown (C). Gray circles, black circles, and empty circles with gray outline indicate low-speed stepping, high-speed stepping, and low-speed stepping+icilin, respectively.

CHAPTER 5-4. DISCUSSION

In this experiment, we demonstrated that TRPM8-mediated cutaneous stimulation combined with low-load treadmill stepping facilitates the activation of large MNs with the activation of cholinergic INs near the central canal. This provides mechanistic insight into the previous finding of increased EMG activity during low-load contraction in humans after stimulation of TRPM8 with menthol (84).

We used icilin as a TRPM8 agonist for cutaneous stimulation in mice (Figure 6). Icilin can cross-activate other TRP channels, such as TRPA1 in vitro (97), while in vivo studies have demonstrated that responses to icilin stimulation in TRPM8$^{-/-}$ mice are reduced to the same extent as that in the control mice (92,98). Thus, icilin stimulation is mediated through TRPM8 in vivo. We believed that icilin is percutaneously absorbed and stimulates TRPM8 in the peripheral sensory nerves (Aδ and C-fibers) (99), followed by induction of c-fos expression in the dorsal horn lamina I and II, the primary site of termination of the thermosensitive and nociceptive sensory afferents (100). Oral or intraperitoneal administration of icilin is reported to produce noxious cold sensations, like wet-dog shakes and jumping behaviors (82,98), but in our experiments, such behaviors were not observed. Therefore we recognize that the application of icilin to the lower limbs stimulates TRPM8-mediated cutaneous afferents but does not extend to induce noxious cold in this study.

We first expected that the number of activated MNs would increase in a stepping speed-dependent manner, however, there was no difference in the results between the Low-speed stp and the High-speed stp groups (Figure 8A). However, the soma size distribution of c-fos^{+} MNs was significantly increased in response to a higher speed (Figure 8B). It suggested that faster stepping speed leads to suppression of the small MNs and activation of the large MNs, promoting preferential recruitment of the larger MUs.

Electromyography signals from the hindlimb muscles in rats during treadmill stepping indicate that faster stepping speed leads to preferential recruitment of the larger MUs (101). It has reported that the small MUs activating at low speeds are suppressed and the large MUs are preferentially activated according to increased exercise speed during bicycling or ankle flexor movements in humans (102,103). These findings suggest that the changes in the MU recruitment patterns are flexible to meet the mechanical demands of each task (104). Thus, the present results obtained from c-fos immunohistochemistry are consistent with the previous findings obtained from electromyography analysis. Furthermore, icilin stimulation induced similar c-fos expression patterns with an increased stepping speed (Figure 8). Despite no change in the stepping speed, TRPM8-mediated cutaneous stimulation may affect the modulation of spinal MN excitability and induce preferential recruitment of the large MUs. Since the application of icilin on sedentary mice did not change the number and the soma size of c-fos^{+} MNs (Figure 8A, Figure S4), the modulation of spinal MN is probably induced by a synergistic effect of TRPM8-mediated cutaneous stimulation and treadmill stepping. The modulation of spinal MN by icilin stimulation is possible to affect the running behavior, because SC on the quadriceps muscle improves the rate of force development during isometric knee extension in human research (79). Quantitative gait analysis of mice treated with icilin is required for future study.

We also found that the number of activated cholinergic INs near the central canal increased following low-speed stepping with icilin stimulation (Figure 9B). These neurons directly synapse onto MNs and regulate their excitability (96,105) via cholinergic presynaptic terminals, C-boutons (106). Acetylcholine (ACh) released from the C-boutons activates M2 muscarinic ACh receptors (M2-mAChRs) on MNs (106) and enhances the MN firing frequency (96). M2-mAChRs are found to be predominantly expressed in the

large MNs, like those innervating mainly the fast medial gastrocnemius muscles (107). Although the details of innervation by INs are still unclear, these findings suggest that large MNs are likely to be modulated via cholinergic INs. Consistent with this hypothesis, our results show that the activation of cholinergic INs positively correlates with the activation of large MNs (Figure 9C). A recent study has shown that treadmill stepping in rats activates these neurons by imposing additional loading by increasing the inclination of the treadmill (89). The authors discuss that increased proprioceptive sensory input by increasing the inclination may affect the activation of the cholinergic INs. Thus TRPM8-mediated sensory input may affect the proprioceptive sensory input and modulate the motor-sensory feedback during exercise. The other possibility is that the TRPM8-mediated sensory input directly activates the cholinergic INs because icilin stimulation tended to slightly increase the number of activated cholinergic INs in the sedentary mice (Figure 9B). Although further study is required to elucidate this mechanism, TRPM8-mediated modulation of MN excitability might be regulated, at least in part, by the cholinergic INs near the central canal.

CHAPTER 6. EXPERIMENT #3

Spinal motor neuron plasticity in hindlimb-unloaded aged mice and treatment of exercise with TRPM8-mediated cutaneous stimulation

CHAPTER 6-1. INTRODUCTION

Frailty is a common clinical syndrome in older adults, which carries an increased risk for poor health outcomes, including falls, incident disability, hospitalization, and mortality (108). It is often characterized by unintentional weight loss, muscle weakness, fatigue, slow walking speed, and low levels of physical activity (109). To prevent frailty, it is important to implement exercises such as strength training or resistance training especially aimed at maintaining and improving muscle strength in lower limbs (110). However, for many elderly people, it is simultaneously necessary to consider the risk of damage to the circulatory system caused by increased blood pressure, or to the musculoskeletal system caused by joint pain. Thus, there is a need to develop training methods that are effective in improving muscle strength even with low loads.

We previously reported that skin cool (SC) sensation mediated by TRPM8 agonist with low-load exercise promotes preferential recruitment of large motor neurons (MNs) (84). Low-load exercise with SC is potentially useful as a new training method for rehabilitation or preventive measures in long-term care for older adults (111). Furthermore, we found that SC with low-load treadmill stepping promoted preferential activation of large MNs which constitute the large motor units in experiment #2. As a mechanism, we found the involvement of cholinergic interneurons (INs) that project directly to the MN cell bodies. Synaptic terminals of these INs are called C-boutons, which releases acetylcholine to excite MNs

(106). As the number of C-boutons decreases with aging (112), C-boutons are expected to be an important target for improving motor function.

In this experiment, we treated aged mice with hindlimb unloading (HU) to induce muscle atrophy, assuming a model for an older adult being frailty or in need of long-term care, and clarified changes in the spinal MN plasticity. In addition, we investigated the effect of exercise with TRPM8-mediated SC on the improvement of motor function and spinal motor control in aged-HU mice.

CHAPTER 6-2. MATERIALS AND METHODS

6-2-1. Animals

Male C57BL/6J mice (young: 12 weeks old and aged: 22 months old) were purchased from The Jackson Laboratory Japan (Kanagawa, Japan) and maintained under controlled conditions (temperature: 23 ± 2 °C; humidity: 55 ± 10%; lighting: 07:00 to 19:00 h). The mice were provided standard chow (CE-2; CLEA Japan, Tokyo, Japan) and ad libitum access to water. All animal experiments were conducted at the Experimental Animal Facility of the Kao Tochigi Institute (Tochigi, Japan) and were approved by the Animal Care Committee of the Kao Corporation (Tokyo, Japan).

6-2-2. Animal Experiment 1

The young and aged mice were randomly divided into two groups, respectively: Young-control (Young-Ctrl, n = 3), Young-HU (Young-HU, n = 4), Aged-Ctrl (n = 4), and Aged-HU (n = 3). The tails of the HU mice were connected to a suspension clip (MTC2014, Yamashita-Giken, Tokushima, Japan), and the hindlimbs were elevated for 2 weeks. The HU mice were able to move 360° with their forelimbs, but could not touch the bottom or sides of the home cage with their hindlimbs. The Ctrl mice were kept sedentary in their home cage.

6-2-3. Animal Experiment 2

After evaluating motor function by beam walking test (**6-2-4)**, young (n = 4) and aged (n = 15) mice were subjected to HU for 2 weeks. After all mice were reloaded, motor function was assessed by beam walking test again. Aged mice were randomly divided into three groups to ensure no differences in body weight and motor function, with sedentary (Sed), treadmill walking (10m/min, 30min/day, five times/week;

Ex), or Ex+SC conditions. The topical application of SC was as described in **5-2-2** using the icilin solution. After the intervention for 2 weeks, motor function was assessed by beam walking test.

6-2-4. Beam walking test

The beam walking test apparatus (SHINFACTORY, Fukuoka, Japan) consisted of a beam (length 80 cm × width 2.2 - 4 cm), two poles supporting the beam at a height of 100 cm above the floor, and a black box. The box is located at the end of the beam. Each mouse was placed at the edge of the beam, and encouraged to walk toward the black box. The time for each mouse walking 50 cm to the black box was measured. The width of the beam was designed to gradually taper from 1.1 mm to 6 mm. Three measurements were performed for each mouse and the average of the two upper scores was calculated. All measurements were blindly performed by a single experimenter who does not know the experimental conditions.

6-2-5. Tissue collection

The spinal cord was isolated and transversely sectioned as described in **5-2-4**, and **5-2-5**.

6-2-6. Immunohistochemistry

Eight sections per individual, randomly obtained from lumbar spinal cord L3-5, were immunostained as described in **5-2-5**. The primary antibodies used in this study included anti-NeuN (MAB377, mouse, 1:1000, EMD Millipore), anti-ChAT (AB114P, goat, 1:300, EMD Millipore), anti-VAChT (ABN100, goat, 1:250, EMD Millipore), and anti-vesicular glutamate transporter 1 (VGLUT1, AB5905, guinea pig, 1:250, EMD, Millipore). The appropriate secondary antibodies conjugated with Alexa Fluor (1:1000, Molecular Probes, Thermo Fisher Scientific) were used.

6-2-7. Analysis of neurons

Digital images were acquired with an all-in-one fluorescence microscope (BZ-X700, Keyence) by Z-stacks with 10–15 μm depth from surface and 1 μm interval, at a magnification of 20X. For quantitative analysis, BZ Analyzer (Keyence) was used to count C-bouton and VGLUT1 spots. C-bouton was determined by quantifying the number of VAChT spots adhering to the contours of NeuN-positive MN cell bodies and dividing by the cell body area per 100 μm^2 (spots/100 μm^2). VGLUT1 spots were analyzed in the same manner. For the above analysis, approximately 50 to 100 MNs were evaluated, and the average value was used as the value for that individual. ChAT-positive cells located in the range of 400 μm width and 300 μm length centering on the central canal were defined as cholinergic INs near the central canal as described in **5-2-6**, and the number of these cells was counted.

6-2-8. Statistical analysis

All data are represented by the mean ± S.E. Differences between multiple groups were tested using one-way ANOVA followed by Tukey's post-hoc test. Comparison of two factors was performed using two-way ANOVA followed by Tukey's post hoc test when a significant interaction was observed. The threshold of significance was set at $p<0.05$. All analysis was performed using Prism 8 statistical software (GraphPad Software, San Diego, CA, USA).

CHAPTER 6-3. RESULTS

6-3-1. Effects of hindlimb unloading on body composition and beam test performance

Neither young nor aged mice lost body weight after 2 weeks of HU (Figure 10A). Consistent with this, HU did not cause the increase in adrenal mass, a marker of stress (113) (Figure 10B). In contrast, soleus and gastrocnemius mass were significantly decreased after HU in both young and aged mice (Figure 10C, D). In young mice, the performance of beam walking test before and after HU was unchanged, but in aged mice, that was significantly worsened after HU (Figure 10E, F).

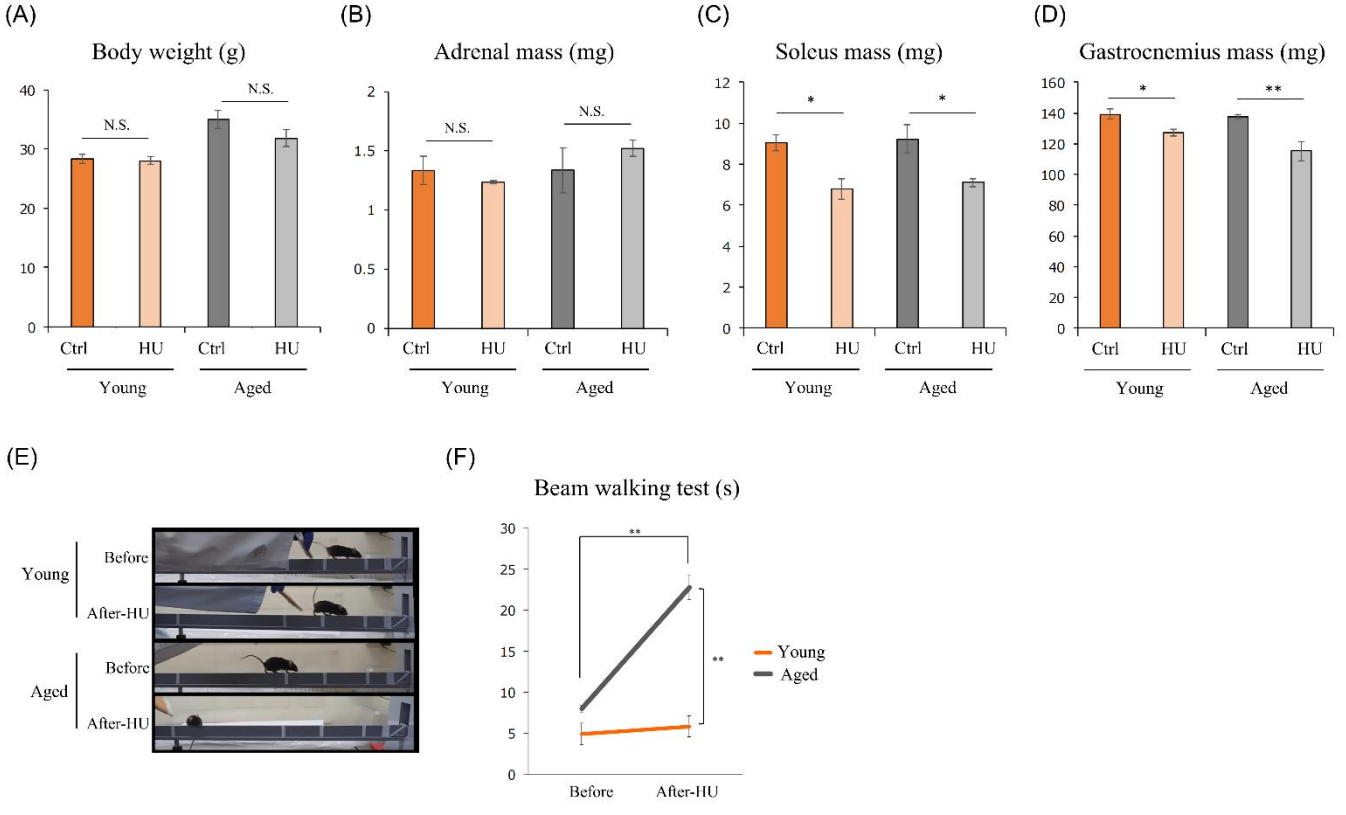

Figure 10. Hindlimb unloading induces muscle atrophy in both young and aged mice, but impaired motor function in only aged mice.

Body weight (A), adrenal mass (B), soleus mass (C), and gastrocnemius mass (D) from 2 week HU mice and their respective controls. Representative images of beam walking test are shown (E). Changes in beam walking test performance before and after HU (F). Data are presented as mean ± SEM (n = 3-4 (A-D), n = 4 (young), n = 15 (aged) (F)). * $p < 0.05$, ** $p < 0.01$ as determined by two-way ANOVA.

6-3-2. Effects of hindlimb unloading on spinal cord neural plasticity

With immunostaining for VAChT, we visualized cholinergic inputs, C-boutons, terminating on MNs innervating hindlimb skeletal muscles. The number of C-boutons was not changed by HU in young mice, but significantly decreased with aging, and was further reduced by HU in aged mice (Figure 11A-C). The number of cholinergic INs near the central canal of the spinal cord decreased with aging (age main effect: $p < 0.05$), but was not affected by HU (Figure 11D-F). Additionally, we examined the impact of aging and HU on glutamatergic inputs. Glutamatergic inputs were visualized with an antibody against VGLUT1. While VGLUT1-spots were present in all regions of the spinal cord, only VGLUT1-spots on MNs in the ventral horn were analyzed. The number of VGLUT1-spots decreased with aging (age main effect: $p < 0.05$), but was not affected by HU (Figure 11G-I).

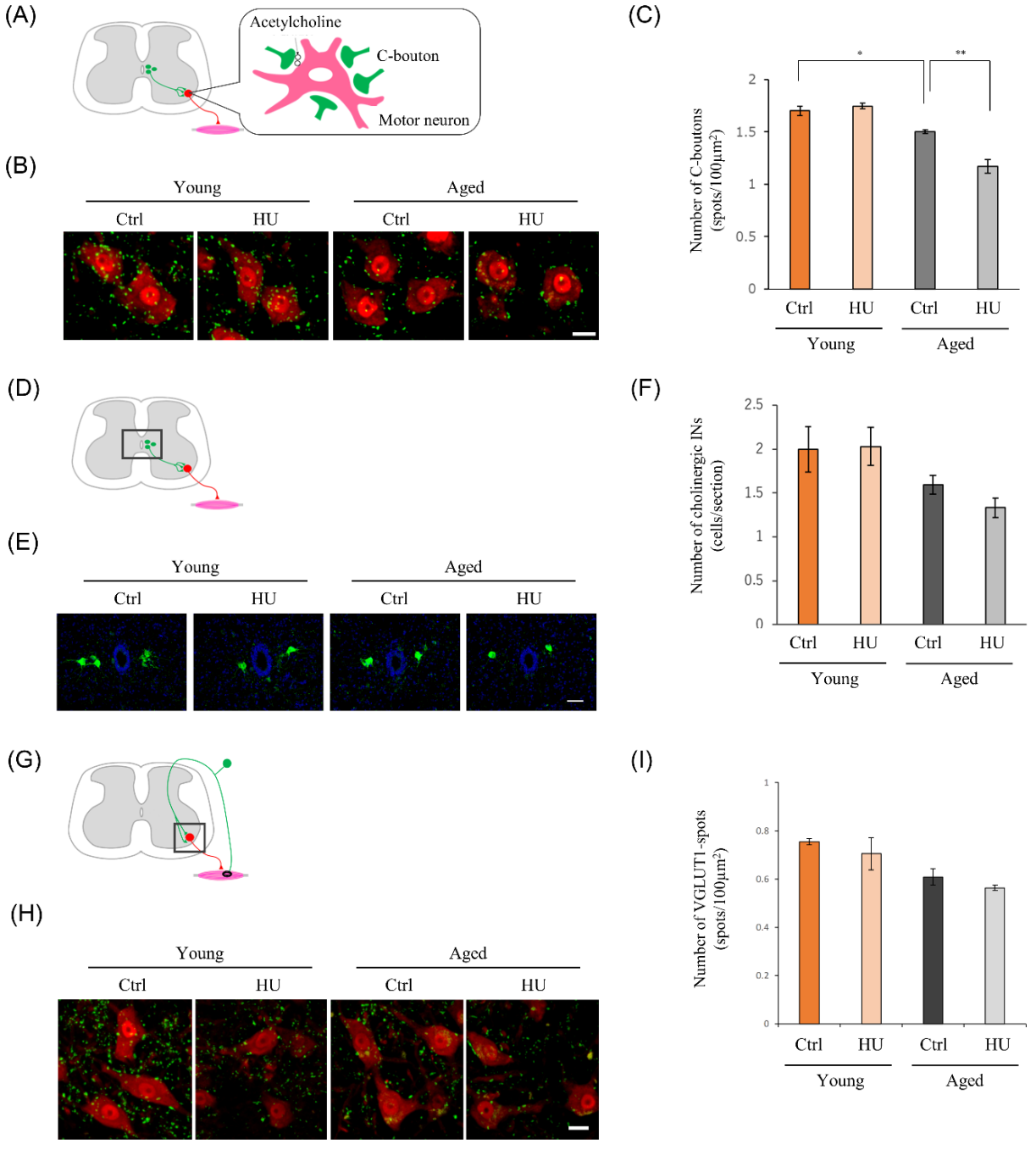
(A)
Acetylcholine
C-bouton
Motor neuron
(B)
Young
Aged
Ctrl
HU
Ctrl
HU
(C)
Number of C-boutons (spots/100μm²)
Ctrl
HU
Ctrl
HU
Young
Aged
(D)
(E)
Young
Aged
Ctrl
HU
Ctrl
HU
(F)
Number of cholinergic INs (cells/section)
Ctrl
HU
Ctrl
HU
Young
Aged
(G)
(H)
Young
Aged
Ctrl
HU
Ctrl
HU
(I)
Number of VGLUT1-spots (spots/100μm²)
Ctrl
HU
Ctrl
HU
Young
Aged

Figure 11. Excitatory synaptic inputs on motor neurons change with aging and hindlimb unloading. Analysis of C-boutons in the ventral horn of the lumbar spinal cord (A). Representative images of C-boutons on the MN soma immunostained with VAChT (green) and NeuN (red) are shown (B). Scale bar = 20 μm. The number of C-boutons is shown for the young-Ctrl, young-HU, aged-Ctrl, aged-HU groups (C). Analysis of cholinergic INs near the central canal (D). Representative images of the cholinergic INs immunostained with ChAT (green) and DAPI (blue) are shown (E). Scale bar = 50 μm. The number of cholinergic INs is shown (F). Analysis of VGLUT1-spots in the ventral horn of the lumbar spinal cord (G). Representative images of VGLUT1-spots on the MN soma immunostained with VGLUT1 (green) and NeuN (red) are shown (H). Scale bar = 20 μm. The number of VGLUT1-spots is shown (I). Data are presented as mean ± SEM (n = 3-4). * $p < 0.05$, ** $p < 0.01$ as determined by two-way ANOVA.

6-3-3. Exercise with TRPM8-mediated cutaneous stimulation facilitates recovery of motor function in reloading aged mice.

Next, aged mice were reloaded after 2 weeks of HU and subjected to a 2-week Ex+SC intervention. Body weight, and soleus and gastrocnemius muscle mass were unchanged between the groups (Figure 12A-C). The beam walking test performance was significantly improved by the Ex+SC group compared to the Sed group (Figure 12D, E). Furthermore, the number of C-boutons was significantly recovered by Ex+SC (Figure 12F, G). Ex alone remained neither changed.

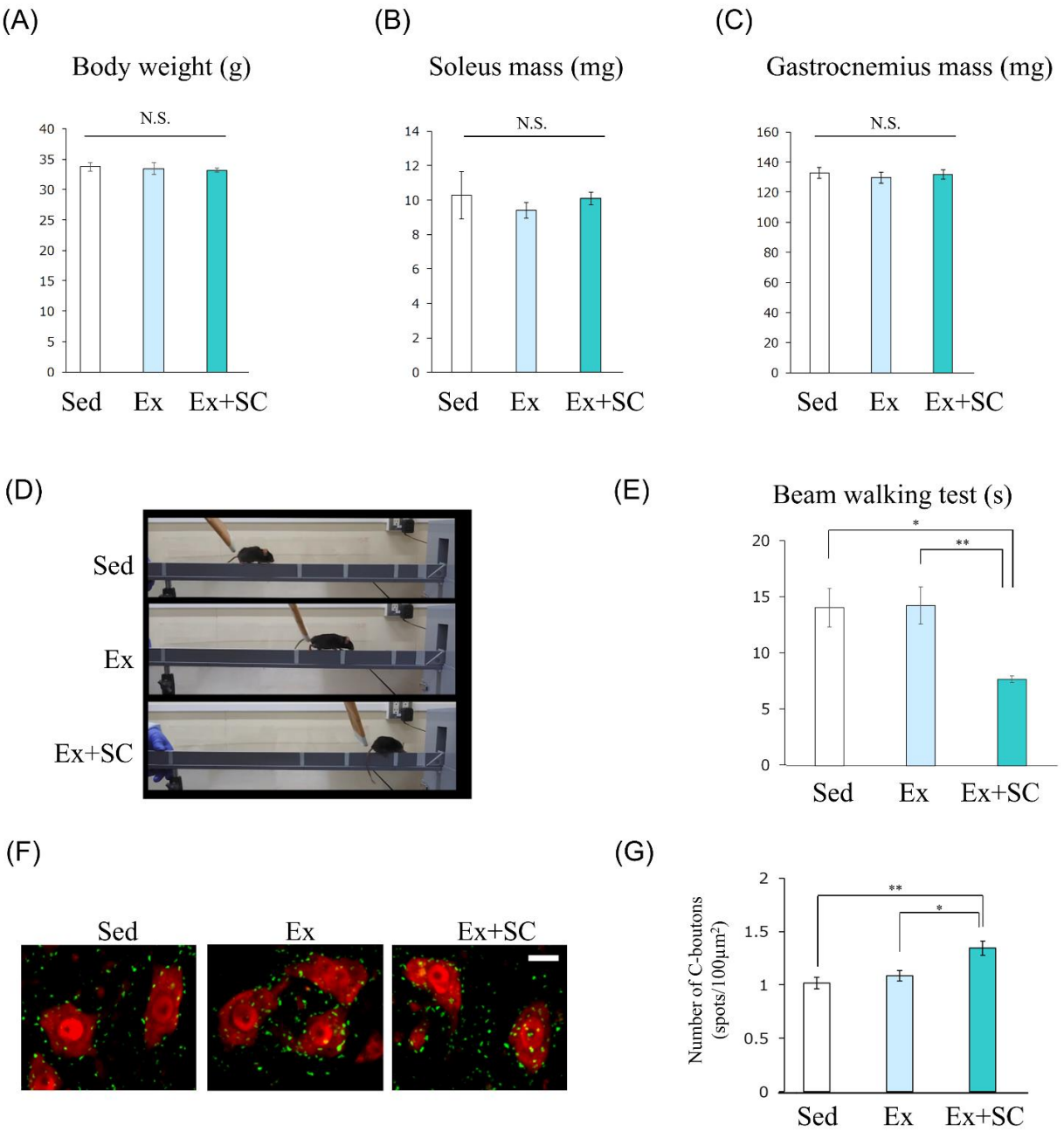
(A)
Body weight (g)
N.S.
40
35
30
25
20
15
10
5
0
Sed
Ex
Ex+SC
(B)
Soleus mass (mg)
N.S.
14
12
10
8
6
4
2
0
Sed
Ex
Ex+SC
(C)
Gastrocnemius mass (mg)
N.S.
160
140
120
100
80
60
40
20
0
Sed
Ex
Ex+SC
(D)
Sed
Ex
Ex+SC
(E)
Beam walking test (s)
*
**
20
15
10
5
0
Sed
Ex
Ex+SC
(F)
Sed
Ex
Ex+SC
(G)
Number of C-boutons (spots/100μm²)
**
*
2
1.5
1
0.5
0
Sed
Ex
Ex+SC

Figure 12. Exercise with TRPM8-mediated skin cooling facilitates recovery of motor function and cholinergic inputs on motor neurons in reloaded aged mice.

Body weight (A), soleus mass (B), and gastrocnemius mass (C) of aged mice after the 2-week intervention. Representative images of beam walking test are shown (D). Changes in beam walking test performance after the 2-week intervention (E). Representative images of C-boutons on the MN soma immunostained with VAChT (green) and NeuN (red) are shown (F). Scale bar = 20 μm. The number of C-boutons is shown for the Sed, Ex, and Ex+SC groups (G). Data are presented as mean ± SEM (n = 4-5). * $p < 0.05$, ** $p < 0.01$ as determined by one way ANOVA.

CHAPTER 6-4. DISCUSSION

In this experiment, we demonstrated that HU reduced the number of C-boutons on MNs in aged mice, with worse beam walking test performance. Recovery from these changes was facilitated through the intervention of low-load treadmill exercise with SC. These findings suggest that changes in C-bouton contribute to spinal motor control and are one of the targets for improving motor function.

HU has been developed as a ground-based unweighting model equivalent to space flight (114) and induces significant atrophy of hindlimb skeletal muscles, especially the soleus muscle. In this experiment, no weight loss or adrenal hypertrophy was observed after 2 weeks of HU (Figure 10A, B), suggesting that stress induced by HU could be negligible for mice. Although muscle atrophy was observed in both young and aged mice (Figure 10C, D), only aged mice showed a significant decrease in motor function (beam walking test) induced by HU (Figure 10E, F). The beam walking test reflects fine motor control and balance function in mice and is often used to evaluate motor dysfunction associated with lesions of the central nervous system and sensory nerves (115). Thus, we next focused on the effects of HU on the spinal nervous system. HU is frequently used as a model to study disuse muscle atrophy, but few reports have examined its effects on the spinal cord (116). First, we analyzed cholinergic INs near the central canal of the spinal cord, which may play an important role in the control of motor units by TRPM8-mediated SC (117). The number of C-boutons projecting to MN somata was reduced by HU only in aged mice (Figure 11C), suggesting that the excitatory synaptic coupling between cholinergic INs and MNs was attenuated. In contrast, the number of glutamatergic presynapses (VGLUT1-spots), that input muscle spindle-derived sensory feedback signals to MN cell bodies (118), decreased with aging but was unchanged by HU (Figure 11D). Although other major interneuron presynapses such as VGLUT2 (glutamatergic) and VGAT

(GABAergic) projecting to MN cell bodies should be analyzed in the future study, the synaptic connections between cholinergic INs and MNs via the C-boutons may be involved in the motor function of aged mice. Recent studies suggest that C-boutons may be a potential therapeutic target for amyotrophic lateral sclerosis and motor dysfunction associated with peripheral nerve injury (119,120). In wild-type mice, gastrocnemius muscle activity increases during swimming compared to walking, but in mice genetically inhibited acetylcholine release from C-bouton, the gastrocnemius muscle activity during swimming is significantly reduced (105). This result suggests that cholinergic inputs to MNs via the C-boutons promote MN firing in a task-dependent manner that requires greater muscle activity. Although the contribution of C-boutons to the beam walking test should be examined in the future study, previous studies have reported that rate of force development (⊿muscle force/⊿time) in older adults is associated with balance function, walking speed, and reduced fall risk (121–123), suggesting that the exerting greater force quickly due to cholinergic inputs could also contribute to the beam walking test performance.

After a 2-week reloading period, the muscle mass tended to recover compared with immediately after HU, but there was no difference between the groups (Figure 12B, C). In contrast, the beam walking test and the number of C-boutons were improved by the intervention of Ex+SC training (Figure 12E, G). The Ex was a low-speed treadmill stepping of 10 m/min, which did not activate the cholinergic INs in Experiment #2, thereby the Ex alone improved neither. Collectively, low-load exercise training with SC by the topical application of TRPM8 agonists enhanced the excitatory synaptic connections between cholinergic INs and MNs, thereby improved motor function. It is necessary to further elucidate the synaptic mechanisms by which the cold sensation influences activating cholinergic INs near the central canal.

CHAPTER 7. GENERAL DISCUSSION

In experiment #1, we demonstrated that Tyr enhanced Leu-induced activation of mTORC1 signaling in C2C12 cells. A similar effect was observed in isolated murine muscle and the skeletal muscles of mice orally administered the amino acids. Other recent studies have reported that Leu, isoleucine, and valine (BCAAs) in combination with alanine at specific ratios enhance BCAA bioavailability and promote anabolic responses in the skeletal muscles (124,125). Thus, the most appropriate amino acid composition for achieving optimal nutritional benefits should be validated in future studies. Our findings may provide important factors to be considered when establishing amino acid combinations suitable for promoting muscle synthesis and may help in the development of nutritional approaches for preventing and treating sarcopenia and frailty. Additional study is required to verify whether long-term intake of protein sources highly contained Leu and Tyr can prevent age-related muscle atrophy in aged mice or older adults. It is also unclear whether the intracellular regulation of mTORC1 by amino acid is maintained in aged skeletal muscle. This would provide a new perspective in addressing anabolic resistance.

In experiment #2, we demonstrated that topical application of a TRPM8 agonist with low-load treadmill stepping promoted preferential activation of large MNs which constitute the large motor units. TRPM8-mediated modulation of the spinal MN excitability may be regulated by cholinergic INs near the central canal. Subsequently, in experiment #3, we demonstrated that repeated TRPM8-mediated cutaneous stimulation with low-load training promoted the excitatory synaptic connections between cholinergic INs and MNs, which should improve motor function in aged mice. These findings could support the possibility of using cutaneous SC input as effective training method for older adults. Recent studies have pointed out that age-related degeneration in the spinal cord is the onset of the decline in physical function (127,128).

The experiment #3 also suggested young mice should have a resilient spinal cord nervous system, since no prominent changes were observed due to HU. In contrast, the nervous system was disrupted in aged mice, probably due to changes in the spinal cord environment with aging. We need to identify the factors which is responsible for regulating the plasticity of spinal cord nervous system including C-boutons in future studies.

Finally, multiple countermeasures for both neurological and skeletal muscle factors are important to address the age-related decline in physical function and muscle atrophy. Certain micronutrients such as plant flavonoids (129) and milk fat globule membrane (130) may also be beneficial in the nutritional management against the age-related deterioration of the neuromuscular system. An integrated exercise and nutrition intervention approach needs to be established for each older individual in the future study.

CHAPTER 8. CONCLUSION

In conclusion, this doctoral thesis tried to understand the mechanisms regulating muscle anabolic response and motor unit recruitment. In experiment #1, we demonstrated that Tyr enhanced Leu-induced activation of mTORC1 signaling. In experiment #2, we demonstrated that topical application of a TRPM8 agonist with low-load treadmill stepping promoted preferential activation of large MNs which constitute the large motor units. Subsequently, in experiment #3, we demonstrated that repeated TRPM8-mediated cutaneous stimulation with low-load training improved motor function in aged mice. The results of the series of experiments provide novel insights into both neurological and skeletal muscle factors contributing to prevent age-related decline in physical function. These findings have the potential for developing effective strategies for rehabilitation or preventive measures in long-term care for older adults.

CHAPTER 9. ACKNOWLEDGMENTS

I would like to express my sincere gratitude to my supervisor, Professor Nobuharu L. Fujii, Associate Professor Yasuko Manabe, and Assistant Professor Yasuro Furuichi, for providing me this precious opportunity to apply for a Ph.D. in their laboratory and for their thoughtful guidance, considerable encouragement, and invaluable discussions. I am also very grateful to Dr. Shin Terada, for his insightful comments and suggestions, Dr. Naoko Goto-inoue, for her advice concerning my previous research.

I would like to thank past and present laboratory members of Biological Science Research at Kao Corporation for their support in matters that involved research.

CHAPTER 10. CONFLICT OF INTERESTS

I am an employee of Kao Corporation. This study was financially supported by Kao Corporation.

CHAPTER 11. REFERENCES

1. Clark BC, Manini TM. Sarcopenia =/= dynapenia. J Gerontol A Biol Sci Med Sci. 2008 Aug;63(8):829–34.

2. Faulkner JA, Larkin LM, Claflin DR, Brooks SV. Age-related changes in the structure and function of skeletal muscles. Clin Exp Pharmacol Physiol. 2007 Nov;34(11):1091–6.

3. Lexell J, Taylor CC, Sjöström M. What is the cause of the ageing atrophy? Total number, size and proportion of different fiber types studied in whole vastus lateralis muscle from 15- to 83-year-old men. J Neurol Sci. 1988 Apr;84(2–3):275–94.

4. Akima H, Kano Y, Enomoto Y, Ishizu M, Okada M, Oishi Y, et al. Muscle function in 164 men and women aged 20--84 yr. Med Sci Sports Exerc. 2001 Feb;33(2):220–6.

5. Janssen I, Heymsfield SB, Wang ZM, Ross R. Skeletal muscle mass and distribution in 468 men and women aged 18-88 yr. J Appl Physiol Bethesda Md 1985. 2000 Jul;89(1):81–8.

6. Skelton DA, Greig CA, Davies JM, Young A. Strength, power and related functional ability of healthy people aged 65-89 years. Age Ageing. 1994 Sep;23(5):371–7.

7. Lexell J. Human aging, muscle mass, and fiber type composition. J Gerontol A Biol Sci Med Sci. 1995 Nov;50 Spec No:11–6.

8. Tomlinson BE, Irving D. The numbers of limb motor neurons in the human lumbosacral cord throughout life. J Neurol Sci. 1977 Nov;34(2):213–9.

9. Kawamura Y, O'Brien P, Okazaki H, Dyck PJ. Lumbar motoneurons of man II: the number and diameter distribution of large- and intermediate-diameter cytons in "motoneuron columns" of spinal cord of man. J Neuropathol Exp Neurol. 1977;36(5):861–70.

10. Luff AR. Age-associated Changes in the Innervation of Muscle Fibers and Changes in the Mechanical Properties of Motor Units. Ann N Y Acad Sci. 1998;854(1):92–101.

11. Manini TM, Hong SL, Clark BC. Aging and muscle: a neuron's perspective. Curr Opin Clin Nutr Metab Care. 2013 Jan;16(1):21–6.

12. Rennie MJ, Edwards RH, Halliday D, Matthews DE, Wolman SL, Millward DJ. Muscle protein synthesis measured by stable isotope techniques in man: the effects of feeding and fasting. Clin Sci Lond Engl 1979. 1982 Dec;63(6):519–23.

13. Phillips SM, Tipton KD, Aarsland A, Wolf SE, Wolfe RR. Mixed muscle protein synthesis and breakdown after resistance exercise in humans. Am J Physiol. 1997 Jul;273(1 Pt 1):E99-107.

14. Biolo G, Maggi SP, Williams BD, Tipton KD, Wolfe RR. Increased rates of muscle protein turnover and amino acid transport after resistance exercise in humans. Am J Physiol. 1995 Mar;268(3 Pt 1):E514-520.

15. Biolo G, Tipton KD, Klein S, Wolfe RR. An abundant supply of amino acids enhances the metabolic effect of exercise on muscle protein. Am J Physiol. 1997 Jul;273(1 Pt 1):E122-129.

16. Rennie MJ. Anabolic resistance: the effects of aging, sexual dimorphism, and immobilization on human muscle protein turnover. Appl Physiol Nutr Metab Physiol Appl Nutr Metab. 2009 Jun;34(3):377–81.

17. Boirie Y, Gachon P, Beaufrère B. Splanchnic and whole-body leucine kinetics in young and elderly men. Am J Clin Nutr. 1997 Feb 1;65(2):489–95.

18. Volpi E, Mittendorfer B, Wolf SE, Wolfe RR. Oral amino acids stimulate muscle protein anabolism in the elderly despite higher first-pass splanchnic extraction. Am J Physiol-Endocrinol Metab. 1999 Sep;277(3):E513–20.

19. Biolo G, Williams BD, Fleming RY, Wolfe RR. Insulin action on muscle protein kinetics and amino acid transport during recovery after resistance exercise. Diabetes. 1999 May;48(5):949–57.

20. Fujita S, Volpi E. Nutrition and sarcopenia of ageing. Nutr Res Rev. 2004 Jun;17(1):69–76.

21. Rasmussen BB, Fujita S, Wolfe RR, Mittendorfer B, Roy M, Rowe VL, et al. Insulin resistance of muscle protein metabolism in aging. FASEB J Off Publ Fed Am Soc Exp Biol. 2006 Apr;20(6):768–9.

22. Fry CS, Drummond MJ, Glynn EL, Dickinson JM, Gundermann DM, Timmerman KL, et al. Aging impairs contraction-induced human skeletal muscle mTORC1 signaling and protein synthesis. Skelet Muscle. 2011 Mar 2;1:11.

23. Markofski MM, Dickinson JM, Drummond MJ, Fry CS, Fujita S, Gundermann DM, et al. Effect of age on basal muscle protein synthesis and mTORC1 signaling in a large cohort of young and older men and women. Exp Gerontol. 2015 May;65:1–7.

24. White Z, White RB, McMahon C, Grounds MD, Shavlakadze T. High mTORC1 signaling is maintained, while protein degradation pathways are perturbed in old murine skeletal muscles in the fasted state. Int J Biochem Cell Biol. 2016 Sep;78:10–21.

25. Wall BT, van Loon LJC. Nutritional strategies to attenuate muscle disuse atrophy. Nutr Rev. 2013 Apr;71(4):195–208.

26. Marshall RN, Smeuninx B, Morgan PT, Breen L. Nutritional Strategies to Offset Disuse-Induced Skeletal Muscle Atrophy and Anabolic Resistance in Older Adults: From Whole-Foods to Isolated Ingredients. Nutrients. 2020 May;12(5):1533.

27. Ma XM, Blenis J. Molecular mechanisms of mTOR-mediated translational control. Nat Rev Mol Cell Biol. 2009 May;10(5):307–18.

28. Tipton KD, Gurkin BE, Matin S, Wolfe RR. Nonessential amino acids are not necessary to stimulate net muscle protein synthesis in healthy volunteers. J Nutr Biochem. 1999 Feb;10(2):89–95.

29. Smith K, Reynolds N, Downie S, Patel A, Rennie MJ. Effects of flooding amino acids on incorporation of labeled amino acids into human muscle protein. Am J Physiol. 1998 Jul;275(1):E73-78.

30. Atherton PJ, Smith K, Etheridge T, Rankin D, Rennie MJ. Distinct anabolic signalling responses to amino acids in C2C12 skeletal muscle cells. Amino Acids. 2010 May;38(5):1533–9.

31. Katsanos CS, Kobayashi H, Sheffield-Moore M, Aarsland A, Wolfe RR. A high proportion of leucine is required for optimal stimulation of the rate of muscle protein synthesis by essential amino acids in the elderly. Am J Physiol Endocrinol Metab. 2006 Aug;291(2):E381-387.

32. Norton LE, Wilson GJ, Layman DK, Moulton CJ, Garlick PJ. Leucine content of dietary proteins is a determinant of postprandial skeletal muscle protein synthesis in adult rats. Nutr Metab. 2012 Jul;9(1):67.

33. Churchward-Venne TA, Burd NA, Mitchell CJ, West DWD, Philp A, Marcotte GR, et al. Supplementation of a suboptimal protein dose with leucine or essential amino acids: effects on myofibrillar protein synthesis at rest and following resistance exercise in men. J Physiol. 2012 Jun;590(11):2751–65.

34. Churchward-Venne TA, Breen L, Di Donato DM, Hector AJ, Mitchell CJ, Moore DR, et al. Leucine supplementation of a low-protein mixed macronutrient beverage enhances myofibrillar protein synthesis in young men: a double-blind, randomized trial. Am J Clin Nutr. 2014 Feb;99(2):276–86.

35. Tang JE, Moore DR, Kujbida GW, Tarnopolsky MA, Phillips SM. Ingestion of whey hydrolysate, casein, or soy protein isolate: effects on mixed muscle protein synthesis at rest and following resistance exercise in young men. J Appl Physiol Bethesda Md 1985. 2009 Sep;107(3):987–92.

36. Burd NA, Yang Y, Moore DR, Tang JE, Tarnopolsky MA, Phillips SM. Greater stimulation of myofibrillar protein synthesis with ingestion of whey protein isolate v. micellar casein at rest and after resistance exercise in elderly men. Br J Nutr. 2012 Sep;108(6):958–62.

37. Wolfson RL, Chantranupong L, Saxton RA, Shen K, Scaria SM, Cantor JR, et al. Sestrin2 is a leucine sensor for the mTORC1 pathway. Science. 2016 Jan;351(6268):43–8.

38. Saxton RA, Knockenhauer KE, Wolfson RL, Chantranupong L, Pacold ME, Wang T, et al. Structural basis for leucine sensing by the Sestrin2-mTORC1 pathway. Science. 2016 Jan;351(6268):53–8.

39. Peng M, Yin N, Li MO. Sestrins function as guanine nucleotide dissociation inhibitors for Rag GTPases to control mTORC1 signaling. Cell. 2014 Sep;159(1):122–33.

40. Chantranupong L, Wolfson RL, Orozco JM, Saxton RA, Scaria SM, Bar-Peled L, et al. The Sestrins interact with GATOR2 to negatively regulate the amino-acid-sensing pathway upstream of mTORC1. Cell Rep. 2014 Oct;9(1):1–8.

41. Xu D, Shimkus KL, Lacko HA, Kutzler L, Jefferson LS, Kimball SR. Evidence for a role for Sestrin1 in mediating leucine-induced activation of mTORC1 in skeletal muscle. Am J Physiol Endocrinol Metab. 2019 May;316(5):E817–28.

42. Nicklin P, Bergman P, Zhang B, Triantafellow E, Wang H, Nyfeler B, et al. Bidirectional transport of amino acids regulates mTOR and autophagy. Cell. 2009 Feb;136(3):521–34.

43. Chantranupong L, Scaria SM, Saxton RA, Gygi MP, Shen K, Wyant GA, et al. The CASTOR Proteins Are Arginine Sensors for the mTORC1 Pathway. Cell. 2016 Mar;165(1):153–64.

44. Gu X, Orozco JM, Saxton RA, Condon KJ, Liu GY, Krawczyk PA, et al. SAMTOR is an S-adenosylmethionine sensor for the mTORC1 pathway. Science. 2017 Nov;358(6364):813–8.

45. Inagaki A, Maruo K, Furuichi Y, Miyatake S, Tamura K, Fujii NL, et al. An improved glucose transport assay system for isolated mouse skeletal muscle tissues. Biosci Biotechnol Biochem. 2016 Nov;80(11):2224–30.

46. Anthony JC, Anthony TG, Kimball SR, Vary TC, Jefferson LS. Orally administered leucine stimulates protein synthesis in skeletal muscle of postabsorptive rats in association with increased eIF4F formation. J Nutr. 2000 Feb;130(2):139–45.

47. Crozier SJ, Kimball SR, Emmert SW, Anthony JC, Jefferson LS. Oral leucine administration stimulates protein synthesis in rat skeletal muscle. J Nutr. 2005 Mar;135(3):376–82.

48. Okahara F, Suzuki J, Hashizume K, Osaki N, Shimotoyodome A. Triterpene alcohols and sterols from rice bran reduce postprandial hyperglycemia in rodents and humans. Mol Nutr Food Res. 2016 Jul;60(7):1521–31.

49. Schmidt EK, Clavarino G, Ceppi M, Pierre P. SUnSET, a nonradioactive method to monitor protein synthesis. Nat Methods. 2009 Apr;6(4):275–7.

50. Goodman CA, Hornberger TA. Measuring protein synthesis with SUnSET: a valid alternative to traditional techniques? Exerc Sport Sci Rev. 2013 Apr;41(2):107–15.

51. Han JM, Jeong SJ, Park MC, Kim G, Kwon NH, Kim HK, et al. Leucyl-tRNA synthetase is an intracellular leucine sensor for the mTORC1-signaling pathway. Cell. 2012 Apr;149(2):410–24.

52. Deldicque L, Sanchez Canedo C, Horman S, De Potter I, Bertrand L, Hue L, et al. Antagonistic effects of leucine and glutamine on the mTOR pathway in myogenic C2C12 cells. Amino Acids. 2008 Jun;35(1):147–55.

53. Areta JL, Hawley JA, Ye JM, Chan MHS, Coffey VG. Increasing leucine concentration stimulates mechanistic target of rapamycin signaling and cell growth in C2C12 skeletal muscle cells. Nutr Res N Y N. 2014 Nov;34(11):1000–7.

54. Koopman R, Wagenmakers AJM, Manders RJF, Zorenc AHG, Senden JMG, Gorselink M, et al. Combined ingestion of protein and free leucine with carbohydrate increases postexercise muscle protein synthesis in vivo in male subjects. Am J Physiol Endocrinol Metab. 2005 Apr;288(4):E645-653.

55. Haegens A, Schols AM, van Essen AL, van Loon LJ, Langen RC. Leucine induces myofibrillar protein accretion in cultured skeletal muscle through mTOR dependent and -independent control of myosin heavy chain mRNA levels. Mol Nutr Food Res. 2012 May;56(5):741–52.

56. Mittendorfer B, Andersen JL, Plomgaard P, Saltin B, Babraj JA, Smith K, et al. Protein synthesis rates in human muscles: neither anatomical location nor fibre-type composition are major determinants. J Physiol. 2005 Feb;563(Pt 1):203–11.

57. Chen J, Ou Y, Luo R, Wang J, Wang D, Guan J, et al. SAR1B senses leucine levels to regulate mTORC1 signalling. Nature. 2021 Aug;596(7871):281–4.

58. Lynch CJ. Role of leucine in the regulation of mTOR by amino acids: revelations from structure-activity studies. J Nutr. 2001 Mar;131(3):861S-865S.

59. Lynch CJ, Fox HL, Vary TC, Jefferson LS, Kimball SR. Regulation of amino acid-sensitive TOR signaling by leucine analogues in adipocytes. J Cell Biochem. 2000 Mar;77(2):234–51.

60. Sato Y, Sato Y, Suzuki R, Obeng K, Yoshizawa F. Leucyl-tRNA synthetase is required for the myogenic differentiation of C2C12 myoblasts, but not for hypertrophy or metabolic alteration of myotubes. Exp Cell Res. 2018 Mar;364(2):184–90.

61. Shimkus KL, Jefferson LS, Gordon BS, Kimball SR. Repressors of mTORC1 act to blunt the anabolic response to feeding in the soleus muscle of a cast-immobilized mouse hindlimb. Physiol Rep. 2018 Oct;6(20):e13891.

62. Zeng N, D'Souza RF, Mitchell CJ, Cameron-Smith D. Sestrins are differentially expressed with age in the skeletal muscle of men: A cross-sectional analysis. Exp Gerontol. 2018 Sep;110:23–34.

63. Segalés J, Perdiguero E, Serrano AL, Sousa-Victor P, Ortet L, Jardí M, et al. Sestrin prevents atrophy of disused and aging muscles by integrating anabolic and catabolic signals. Nat Commun. 2020 Jan;11(1):189.

64. Zeng N, D'Souza RF, Figueiredo VC, Markworth JF, Roberts LA, Peake JM, et al. Acute resistance exercise induces Sestrin2 phosphorylation and p62 dephosphorylation in human skeletal muscle. Physiol Rep. 2017 Dec;5(24):e13526.

65. Crisol BM, Lenhare L, Gaspar RS, Gaspar RC, Muñoz VR, da Silva ASR, et al. The role of physical exercise on Sestrin1 and 2 accumulations in the skeletal muscle of mice. Life Sci. 2018 Feb;194:98–103.

66. Mitchell CJ, Churchward-Venne TA, Cameron-Smith D, Phillips SM. What is the relationship between the acute muscle protein synthesis response and changes in muscle mass? J Appl Physiol Bethesda Md 1985. 2015 Feb;118(4):495–7.

67. Henneman E, Somjen G, Carpenter DO. FUNCTIONAL SIGNIFICANCE OF CELL SIZE IN SPINAL MOTONEURONS. J Neurophysiol. 1965 May;28:560–80.

68. Milner-Brown HS, Stein RB, Yemm R. The orderly recruitment of human motor units during voluntary isometric contractions. J Physiol. 1973 Apr;230(2):359–70.

69. Cope TC, Clark BD. Are there Important Exceptions to the Size Principle of α-Motoneurone Recruitment? In: Taylor A, Gladden MH, Durbaba R, editors. Alpha and Gamma Motor Systems [Internet]. Boston, MA: Springer US; 1995 [cited 2023 Dec 23]. p. 71–8. Available from: https://doi.org/10.1007/978-1-4615-1935-5_15

70. Garnett R, Stephens JA. The reflex responses of single motor units in human first dorsal interosseous muscle following cutaneous afferent stimulation. J Physiol. 1980 Jun;303:351–64.

71. Masakado Y, Kamen G, De Luca CJ. Effects of percutaneous stimulation on motor unit firing behavior in man. Exp Brain Res. 1991;86(2):426–32.

72. Nielsen J, Kagamihara Y. Differential projection of the sural nerve to early and late recruited human tibialis anterior motor units: change of recruitment gain. Acta Physiol Scand. 1993 Apr;147(4):385–401.

73. Zehr EP. Training-induced adaptive plasticity in human somatosensory reflex pathways. J Appl Physiol. 2006 Dec;101(6):1783–94.

74. Seo NJ, Kosmopoulos ML, Enders LR, Hur P. Effect of remote sensory noise on hand function post stroke. Front Hum Neurosci. 2014;8:934.

75. van der Salm A, Veltink PH, Ijzerman MJ, Groothuis-Oudshoorn KC, Nene AV, Hermens HJ. Comparison of electric stimulation methods for reduction of triceps surae spasticity in spinal cord injury. Arch Phys Med Rehabil. 2006 Feb;87(2):222–8.

76. Winkel J, Jørgensen K. Significance of skin temperature changes in surface electromyography. Eur J Appl Physiol. 1991;63(5):345–8.

77. Yona M. Effects of cold stimulation of human skin on motor unit activity. Jpn J Physiol. 1997 Aug;47(4):341–8.

78. Sugawara H, Shimose R, Tadano C, Muro M. Skin Cold Stimulation of the Dermatome Modulates Activation of the Quadriceps. J Phys Ther Sci. 2012;24(2):169–74.

79. Shimose R, Ushigome N, Tadano C, Sugawara H, Yona M, Matsunaga A, et al. Increase in rate of force development with skin cooling during isometric knee extension. J Electromyogr Kinesiol Off J Int Soc Electrophysiol Kinesiol. 2014 Dec;24(6):895–901.

80. Tominaga M, Caterina MJ. Thermosensation and pain. J Neurobiol. 2004 Oct;61(1):3–12.

81. Peier AM, Moqrich A, Hergarden AC, Reeve AJ, Andersson DA, Story GM, et al. A TRP channel that senses cold stimuli and menthol. Cell. 2002 Mar;108(5):705–15.

82. Wei ET, Seid DA. AG-3-5: a chemical producing sensations of cold. J Pharm Pharmacol. 1983 Feb;35(2):110–2.

83. McKemy DD, Neuhausser WM, Julius D. Identification of a cold receptor reveals a general role for TRP channels in thermosensation. Nature. 2002 Mar;416(6876):52–8.

84. Tokunaga T, Sugawara H, Tadano C, Muro M. Effect of stimulation of cold receptors with menthol on EMG activity of quadriceps muscle during low load contraction. Somatosens Mot Res. 2017 Jun;34(2):85–91.

85. Jasmin L, Gogas KR, Ahlgren SC, Levine JD, Basbaum AI. Walking evokes a distinctive pattern of Fos-like immunoreactivity in the caudal brainstem and spinal cord of the rat. Neuroscience. 1994 Jan;58(2):275–86.

86. Dai X, Noga BR, Douglas JR, Jordan LM. Localization of spinal neurons activated during locomotion using the c-fos immunohistochemical method. J Neurophysiol. 2005 Jun;93(6):3442–52.

87. Omori T, Kawashima H, Kizuka T, Ohiwa N, Tateoka M, Soya H. Increased c-fos gene expression in alpha motoneurons in rat loaded hindlimb muscles with inclined locomotion. Neurosci Lett. 2005 Nov;389(1):25–9.

88. Ahn SN, Guu JJ, Tobin AJ, Edgerton VR, Tillakaratne NJK. Use of c-fos to identify activity-dependent spinal neurons after stepping in intact adult rats. Spinal Cord. 2006 Sep;44(9):547–59.

89. Tillakaratne NJK, Duru P, Fujino H, Zhong H, Xiao MS, Edgerton VR, et al. Identification of interneurons activated at different inclines during treadmill locomotion in adult rats. J Neurosci Res. 2014 Dec;92(12):1714–22.

90. Stepien AE, Tripodi M, Arber S. Monosynaptic rabies virus reveals premotor network organization and synaptic specificity of cholinergic partition cells. Neuron. 2010 Nov;68(3):456–72.

91. Jovanovic K, Pastor AM, O'Donovan MJ. The use of PRV-Bartha to define premotor inputs to lumbar motoneurons in the neonatal spinal cord of the mouse. PloS One. 2010 Jul;5(7):e11743.

92. Knowlton WM, Bifolck-Fisher A, Bautista DM, McKemy DD. TRPM8, but not TRPA1, is required for neural and behavioral responses to acute noxious cold temperatures and cold-mimetics in vivo. Pain. 2010 Aug;150(2):340–50.

93. Kaplan A, Spiller KJ, Towne C, Kanning KC, Choe GT, Geber A, et al. Neuronal matrix metalloproteinase-9 is a determinant of selective neurodegeneration. Neuron. 2014 Jan;81(2):333–48.

94. Müller D, Cherukuri P, Henningfeld K, Poh CH, Wittler L, Grote P, et al. Dlk1 promotes a fast motor neuron biophysical signature required for peak force execution. Science. 2014 Mar;343(6176):1264–6.

95. Huang A, Noga BR, Carr PA, Fedirchuk B, Jordan LM. Spinal cholinergic neurons activated during locomotion: localization and electrophysiological characterization. J Neurophysiol. 2000 Jun;83(6):3537–47.

96. Miles GB, Hartley R, Todd AJ, Brownstone RM. Spinal cholinergic interneurons regulate the excitability of motoneurons during locomotion. Proc Natl Acad Sci U S A. 2007 Feb;104(7):2448–53.

97. Sherkheli MA, Vogt-Eisele AK, Bura D, Beltrán Márques LR, Gisselmann G, Hatt H. Characterization of selective TRPM8 ligands and their structure activity response (S.A.R) relationship. J Pharm Pharm Sci Publ Can Soc Pharm Sci Soc Can Sci Pharm. 2010;13(2):242–53.

98. Colburn RW, Lubin ML, Stone DJ, Wang Y, Lawrence D, D'Andrea MR, et al. Attenuated cold sensitivity in TRPM8 null mice. Neuron. 2007 May;54(3):379–86.

99. Kobayashi K, Fukuoka T, Obata K, Yamanaka H, Dai Y, Tokunaga A, et al. Distinct expression of TRPM8, TRPA1, and TRPV1 mRNAs in rat primary afferent neurons with adelta/c-fibers and colocalization with trk receptors. J Comp Neurol. 2005 Dec;493(4):596–606.

100. Julius D, Basbaum AI. Molecular mechanisms of nociception. Nature. 2001 Sep;413(6852):203–10.

101. Hodson-Tole EF, Wakeling JM. Motor unit recruitment patterns 1: responses to changes in locomotor velocity and incline. J Exp Biol. 2008 Jun;211(Pt 12):1882–92.

102. Citterio G, Agostoni E. Selective activation of quadriceps muscle fibers according to bicycling rate. J Appl Physiol. 1984 Aug;57(2):371–9.

103. Tamaki H, Kitada K, Akamine T, Sakou T, Kurata H. Electromyogram patterns during plantarflexions at various angular velocities and knee angles in human triceps surae muscles. Eur J Appl Physiol. 1997;75(1):1–6.

104. Bawa PNS, Jones KE, Stein RB. Assessment of size ordered recruitment. Front Hum Neurosci. 2014;8:532.

105. Zagoraiou L, Akay T, Martin JF, Brownstone RM, Jessell TM, Miles GB. A cluster of cholinergic premotor interneurons modulates mouse locomotor activity. Neuron. 2009 Dec;64(5):645–62.

106. Witts EC, Zagoraiou L, Miles GB. Anatomy and function of cholinergic C bouton inputs to motor neurons. J Anat. 2014 Jan;224(1):52–60.

107. Hellström J, Oliveira ALR, Meister B, Cullheim S. Large cholinergic nerve terminals on subsets of motoneurons and their relation to muscarinic receptor type 2. J Comp Neurol. 2003 Jun;460(4):476–86.

108. Xue QL. The frailty syndrome: definition and natural history. Clin Geriatr Med. 2011 Feb;27(1):1–15.

109. Fried LP, Tangen CM, Walston J, Newman AB, Hirsch C, Gottdiener J, et al. Frailty in older adults: evidence for a phenotype. J Gerontol A Biol Sci Med Sci. 2001 Mar;56(3):M146-156.

110. Nelson ME, Rejeski WJ, Blair SN, Duncan PW, Judge JO, King AC, et al. Physical activity and public health in older adults: recommendation from the American College of Sports Medicine and the American Heart Association. Med Sci Sports Exerc. 2007 Aug;39(8):1435–45.

111. Tokunaga T, Tadano C, Muro M, Sugawara H. Menthol-induced cutaneous stimulation combined with self-paced walking training improves knee extension performance in untrained older healthy females. J Phys Ther Sci. 2020 Apr;32(4):269–76.

112. Maxwell N, Castro RW, Sutherland NM, Vaughan KL, Szarowicz MD, de Cabo R, et al. α-Motor neurons are spared from aging while their synaptic inputs degenerate in monkeys and mice. Aging Cell. 2018 Apr;17(2):e12726.

113. Ferreira JA, Crissey JM, Brown M. An alternant method to the traditional NASA hindlimb unloading model in mice. J Vis Exp JoVE. 2011 Mar;(49):2467.

114. Morey-Holton ER, Globus RK. Hindlimb unloading rodent model: technical aspects. J Appl Physiol Bethesda Md 1985. 2002 Apr;92(4):1367–77.

115. Luong TN, Carlisle HJ, Southwell A, Patterson PH. Assessment of motor balance and coordination in mice using the balance beam. J Vis Exp JoVE. 2011 Mar;(49):2376.

116. Chelyshev YA, Muhamedshina YO, Povysheva TV, Shaymardanova GF, Rizvanov AA, Nigmetzyanova MV, et al. Characterization of spinal cord glial cells in a model of hindlimb unloading in mice. Neuroscience. 2014 Nov;280:328–39.

117. Tamura K, Sugita S, Tokunaga T, Minegishi Y, Ota N. TRPM8-mediated cutaneous stimulation modulates motor neuron activity during treadmill stepping in mice. J Physiol Sci JPS. 2019 Nov;69(6):931–8.

118. Alvarez FJ, Titus-Mitchell HE, Bullinger KL, Kraszpulski M, Nardelli P, Cope TC. Permanent central synaptic disconnection of proprioceptors after nerve injury and regeneration. I. Loss of VGLUT1/IA synapses on motoneurons. J Neurophysiol. 2011 Nov;106(5):2450–70.

119. Landoni LM, Myles JR, Wells TL, Mayer WP, Akay T. Cholinergic modulation of motor neurons through the C-boutons are necessary for the locomotor compensation for severe motor neuron loss during amyotrophic lateral sclerosis disease progression. Behav Brain Res. 2019 Sep;369:111914.

120. Salvany S, Casanovas A, Tarabal O, Piedrafita L, Hernández S, Santafé M, et al. Localization and dynamic changes of neuregulin-1 at C-type synaptic boutons in association with motor neuron injury and repair. FASEB J Off Publ Fed Am Soc Exp Biol. 2019 Jul;33(7):7833–51.

121. Chang SHJ, Mercer VS, Giuliani CA, Sloane PD. Relationship between hip abductor rate of force development and mediolateral stability in older adults. Arch Phys Med Rehabil. 2005 Sep;86(9):1843–50.

122. Clark DJ, Manini TM, Fielding RA, Patten C. Neuromuscular determinants of maximum walking speed in well-functioning older adults. Exp Gerontol. 2013 Mar;48(3):358–63.

123. Pijnappels M, van der Burg PJCE, Reeves ND, van Dieën JH. Identification of elderly fallers by muscle strength measures. Eur J Appl Physiol. 2008 Mar;102(5):585–92.

124. Mantuano P, Bianchini G, Cappellari O, Boccanegra B, Conte E, Sanarica F, et al. Ergogenic Effect of BCAAs and L-Alanine Supplementation: Proof-of-Concept Study in a Murine Model of Physiological Exercise. Nutrients. 2020 Jul;12(8):2295.

125. Mantuano P, Boccanegra B, Bianchini G, Cappellari O, Tulimiero L, Conte E, et al. Branched-Chain Amino Acids and Di-Alanine Supplementation in Aged Mice: A Translational Study on Sarcopenia. Nutrients. 2023 Jan;15(2):330.

126. Gorissen SHM, Crombag JJR, Senden JMG, Waterval WAH, Bierau J, Verdijk LB, et al. Protein content and amino acid composition of commercially available plant-based protein isolates. Amino Acids. 2018 Dec;50(12):1685–95.

127. Giorgetti E, Panesar M, Zhang Y, Joller S, Ronco M, Obrecht M, et al. Modulation of Microglia by Voluntary Exercise or CSF1R Inhibition Prevents Age-Related Loss of Functional Motor Units. Cell Rep. 2019 Nov;29(6):1539-1554.e7.

128. Piekarz KM, Bhaskaran S, Sataranatarajan K, Street K, Premkumar P, Saunders D, et al. Molecular changes associated with spinal cord aging. GeroScience. 2020 Apr;42(2):765–84.

129. Gras S, Blasco A, Mòdol-Caballero G, Tarabal O, Casanovas A, Piedrafita L, et al. Beneficial effects of dietary supplementation with green tea catechins and cocoa flavanols on aging-related regressive changes in the mouse neuromuscular system. Aging. 2021 Jul;13(14):18051–93.

130. Sugita S, Tamura K, Yano M, Minegishi Y, Ota N. The Impact of Milk Fat Globule Membrane with Exercise on Age-Related Degeneration of Neuromuscular Junctions. Nutrients. 2021 Jul;13(7):2310.

CHAPTER12. APPENDICES

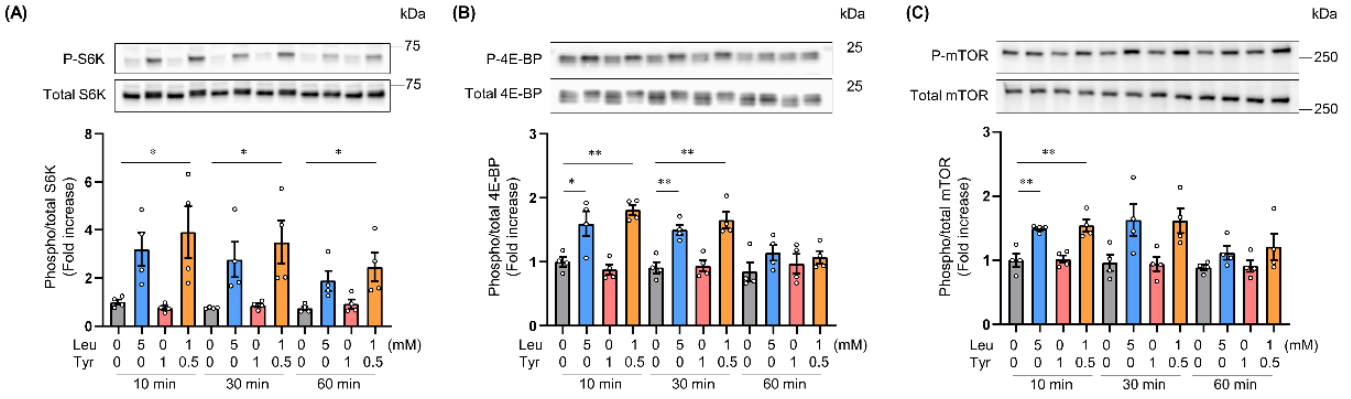

Supplemental figure 1. Time course response of leucine and tyrosine in the anabolic signaling pathway in C2C12 myoblasts.

Phosphorylation of S6K (Thr389) (A), 4E-BP (Thr37/46) (B), and mTOR (Ser2448) (C) 10–60 min after stimulation with Leu and/or Tyr in C2C12 myoblasts on day 1 post-differentiation (n = 4). All data is shown as fold change to Ctrl (0 mM Leu and 0 mM Tyr) at 10 min. Data are presented as the mean ± SEM. Circles represent individual values. *p < 0.05, **p < 0.01 vs. Ctrl as determined by one-way ANOVA.

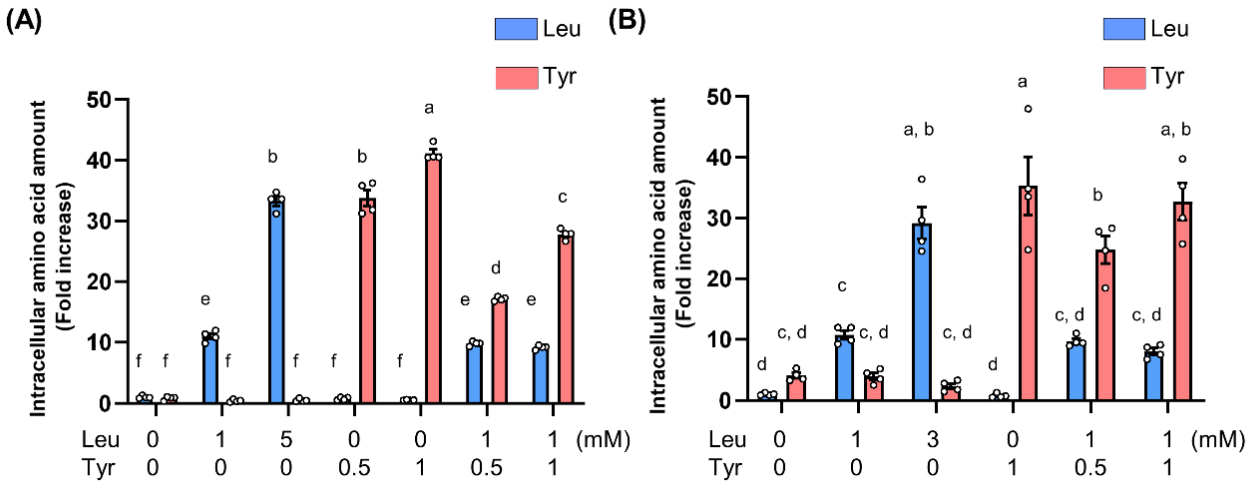

Supplemental figure 2. Measurement of intracellular free amino acid levels following exposure to leucine and tyrosine.

Intracellular free Leu and Tyr levels in (A) C2C12 myoblasts and (B) isolated muscle (EDL) were determined by LC-MS/MS. Measurements of the isolated muscle were corrected for the weight of the muscle brought in. All values are presented relative to the amount of Leu in the control group. Data are presented as the mean ± SEM (n = 4). Circles represent individual values. Different letters (a–f) indicated significant differences ($p < 0.05$) as determined by one-way ANOVA.

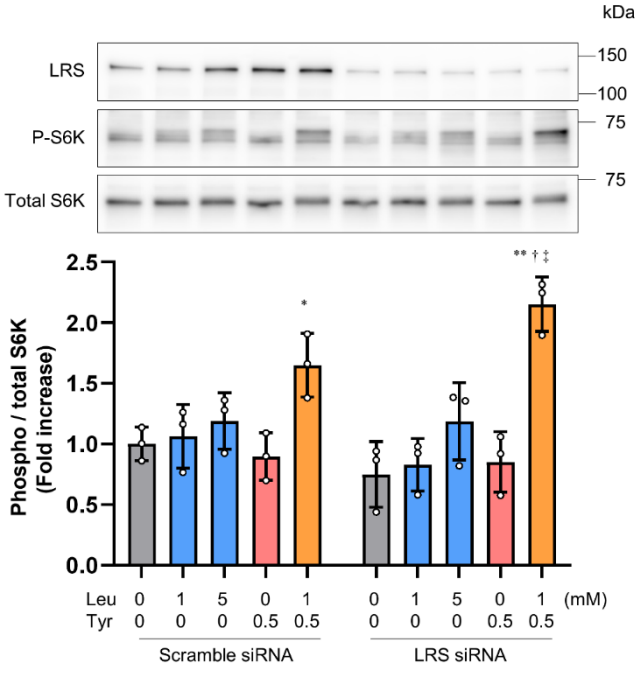

Supplemental figure 3. Effect of LRS expression suppression on leucine and tyrosine-induced S6K phosphorylation.

S6K phosphorylation (Thr389) in response to 15 min of stimulation with Leu and/or Tyr under downregulated LRS expression by siRNA transfection in C2C12 myoblasts on day 1 post-differentiation. Data are presented as the mean ± SEM (n = 3). Circles represent individual values. *p < 0.05 vs. Ctrl (Scr siRNA). ** p < 0.01 vs Ctrl (LRS siRNA). † p < 0.01 vs. 1 mM Leu (LRS siRNA). ‡ p < 0.01 vs. 5 mM Leu (LRS siRNA) as determined by two-way ANOVA.

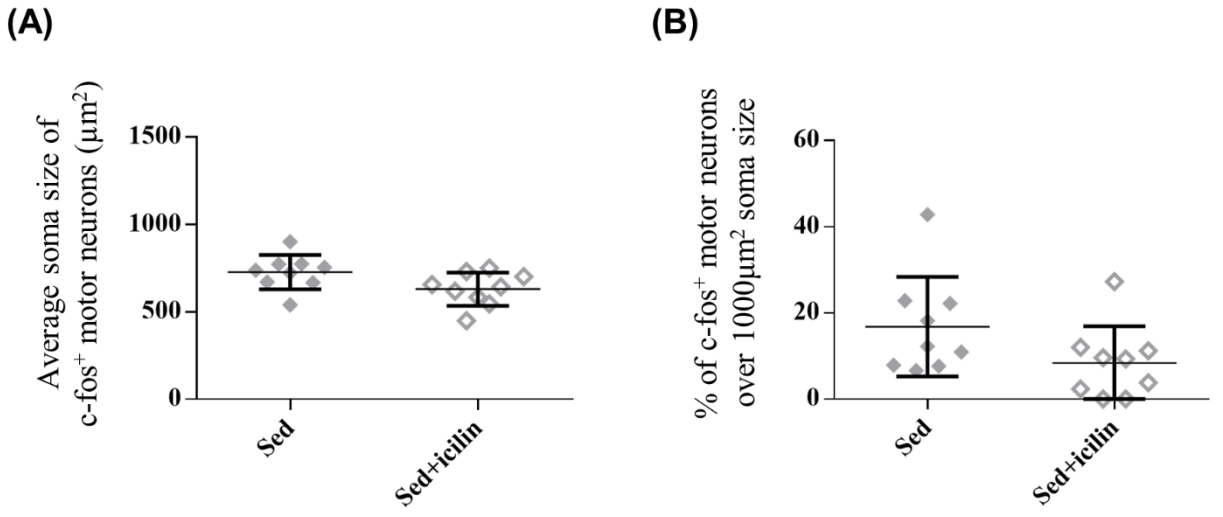

Supplemental figure 4. Application of icilin on sedentary mice does not change the soma size of c-fos$^+$ MNs.

Quantitative results of c-fos$^+$ MNs in immunostained images of the spinal cord are shown for Sed and Sed+icilin groups. The average soma size of the total c-fos$^+$ MNs and the percentage of large soma size (≥ 1000 μm^2) of the c-fos$^+$ MNs are shown in (A) and (B), respectively. Each symbol represents an individual mouse. The horizontal lines indicate the mean values. Data are represented as the means ± S.D.